

Summertime Precipitation Regimes Associated with the Sea Breeze and Land Breeze in Southern Mississippi and Eastern Louisiana

CHRISTOPHER M. HILL, PATRICK J. FITZPATRICK, JAMES H. CORBIN, YEE H. LAU
AND SACHIN K. BHATE

Northern Gulf Institute, Mississippi State University, Stennis Space Center, Mississippi

(Manuscript received 29 July 2009, in final form 4 May 2010)

ABSTRACT

This study assesses the monthly climatology of the timing and placement of convective precipitation events induced by sea and land breezes in the Louisiana–Mississippi–Alabama region, and determines possible reasons for the monthly differences. These objectives were achieved through surface wind climatologies and radar composites from 2003 to 2005, supplemented by statistically significant tests. It is shown that June had an easterly–southeasterly wind regime, whereas July and August featured more southerly flow. These wind regimes may have influenced monthly diurnal wind patterns along the coast. While all months showed a typical pattern of sea-breeze evolution, the land breeze demonstrated monthly variations off the Mississippi and Louisiana coasts. July and August feature a westerly land breeze from Louisiana, while the Mississippi land breeze was stronger in August than in July. A daily wind speed minimum offshore from Mississippi indicates a local transition of influence from the land breeze to the sea breeze, and precedes the peak of the sea breeze at the coastline by about 2 h. During the nighttime hours, radar composites show that precipitation is most prevalent offshore of the Louisiana and Mississippi coastline. By 1100 central daylight time (CDT), precipitation is observed over coastal regions. Local afternoon precipitation is widespread throughout the inland areas, while precipitation is minimal offshore. Statistical significance tests show that areal precipitation coverage (APC) increases in mid- to late summer on the Mississippi coast are due to higher precipitable water and, to a lesser extent, additional CAPE. Greater offshore APC in July and August results from the influence of the local land-breeze setup. Convergence of a land breeze from eastern Louisiana and a stronger land breeze from Mississippi provides the additional lift needed to generate convection over a greater area.

1. Introduction

The sea-breeze circulation (SBC) has long been recognized as a significant mesoscale phenomenon affecting weather conditions throughout coastal regions of the world. According to the early works of Haurwitz (1947) and Neumann (1951), the extent to which the discrete, forward-propagating surface boundary of the SBC—known as the sea-breeze front (SBF; see Table 1 for a list of the key acronyms used in this paper)—migrates inland, and the manner in which it is oriented relative to the coastline, depends on 1) the temperature gradient between land and water, 2) the prevailing boundary layer flow, 3) land elevation, and 4) the shape of the coastline.

Regional variations in coastal geography and topography allow the SBC to take on different forms. Specialized numerical models have been designed to simulate the SBC for specific locations, accounting for the intricate effects of coastal geography and topography (McPherson 1970; Pielke 1974; Anthes 1978; Steyn and Mckendry 1988; Arriitt 1989). Modern mesoscale models also qualitatively capture regional features of the SBC (Case et al. 2002; Colby 2004; Etherton and Santos 2008). Islands (Ramis et al. 1990), peninsulas (Wilson and Megenhardt 1997), mountainous coasts (Banta et al. 1993; Lu and Turco 1994), and lake/river breezes (Physick and Byron-Scott 1977; Simpson 1994) all alter SBCs and their associated precipitations patterns. However, fewer studies have investigated the land–sea breeze regime using land and offshore in situ observations (Hawkins 1977; Sheng et al. 2009) or with radar data. In particular, few climatology studies exist that document the SBC and land-breeze circulation (LBC) cycle along the north-central

Corresponding author address: Christopher M. Hill, Northern Gulf Institute, Bldg. 1103, Rm. 108, Mississippi State University, Stennis Space Center, MS 39529.
E-mail: hillcm@ngi.msstate.edu

TABLE 1. Key acronyms and abbreviations used in the article.

Acronym	Expansion
AL	Alabama
APC	Areal precipitation coverage
CAPE	Convective available potential energy
CDT	Central daylight time (UTC - 5 h)
KI	K index
LA	Louisiana
LBC	Land-breeze circulation
MS	Mississippi
NCGC	North-central Gulf of Mexico
NWS	National Weather Service
PW	Precipitable water
RAWS	Remote Automated Weather Stations
SBC	Sea-breeze circulation
SBF	Sea-breeze front
SLB	Sea and/or land breeze

coast of the Gulf of Mexico (hereafter NCGC) using such a network. Regional lightning studies present 24-h (Reap 1994) and annual (Steiger and Orville 2003) flash data along the NCGC (which serve as a surrogate for convection) but do not convey the daily precipitation cycles. This paper documents monthly wind and precipitation patterns in this region associated with the SBC and LBC using inland and offshore in situ data supplemented by radar data. The cause of the monthly precipitation variations is also postulated from wind and thermodynamic data.

During the summertime, the semipermanent Bermuda high anticyclone over the western Atlantic Ocean transports warm, moist air from over the Gulf of Mexico throughout the southeastern United States. With a moist, unstable air mass in place, an SBF encounters dynamic perturbations of the boundary layer, such as horizontal convective rolls, thunderstorm outflow boundaries, or small lake or river breezes; unstable air parcels are mechanically lifted; and convective cells are initiated (Fovell 2005; Case et al. 2005; Wakimoto and Atkins 1994; Atkins et al. 1995). Hence, the NCGC observes frequent thunderstorm activity during the summer. The position and orientation of an SBF will determine the placement of the associated convective cells, and the cells will generally propagate with the SBF. In turn, the placement and orientation of the SBF along the NCGC can be dependent on the direction of the prevailing, lower-tropospheric flow (Medlin and Croft 1998; Smith et al. 2005; Lu et al. 2006). The presence of the prevailing southerly (northerly) flow typically leads to greater (less) inland migration of the SBF and therefore greater (less) areal coverage of convection along the NCGC. Conversely, a stronger (weaker) SBC exists within prevailing northerly (southerly) flow.

An LBC is observed during the nighttime and within a few hours after dawn. The cross-shore temperature gradient associated with the LBC is less than that associated

with the SBC; hence, the LBC is weaker. As with the SBC, convection can be observed with convergent flow within an LBC; the convection within an LBC is primarily situated over water (Neumann 1951; McPherson 1970). Given the right-angular configuration of the Louisiana–Mississippi coastline, the consequent orientation of cross-shore temperature gradients along the coast, and the nighttime decoupling of boundary layer flow over land from the prevailing synoptic wind, a significant land-breeze front (LBF) may emerge from the Mississippi coast and converge with surface-level synoptic flow over the Mississippi–Alabama Shelf region of the Gulf of Mexico, resulting in the development of clustered convection along the LBF. The orthogonal convergence of the Mississippi LBF with another LBF over eastern Louisiana is an alternative mechanism by which clustered convection may develop.

This paper is the result of data analysis spanning three years that depicts the summertime SBC and LBC, and associated convective precipitation, over coastal areas of Mississippi and Louisiana. One purpose of this study is to assess the monthly climatology of the timing and placement of convective precipitation events induced by sea and land breezes in the NCGC region. Another goal is to ascertain the reasons that these monthly differences exist. Both objectives are pursued using graphical analysis and statistical significance tests of rain coverage, wind patterns, and thermodynamic parameters. Since the skill of the operational models in predicting the timing and location of sea–land-breeze convection is low (Case et al. 2002), a secondary intent is to provide local forecasters, who must still rely solely on current observations and nowcasting, guidance from radar pattern recognition and sounding variables. Both goals are assisted with monthly radar composites and multiple-regression analysis. Section 2 details the methodology used in this study. Section 3 presents the results of the study. Section 4 provides a discussion of the results and our conclusions.

2. Methodology

Hourly observations of wind direction, wind speed, pressure, temperature, and dewpoint temperature are examined from 21 surface stations and 6 buoys in the region of interest, as are 12-h observations of wind, temperature, and dewpoint temperature from the Slidell, Louisiana (KLIX), rawinsonde station (see Fig. 1 and Table 2), for June, July, and August (JJA) of 2003–05. Additionally, the following parameters were derived from the rawinsonde observations: convective available potential energy (CAPE), K index (KI), and precipitable water (PW) integrated between 1000 and 300 hPa. The surface stations selected are National Weather Service

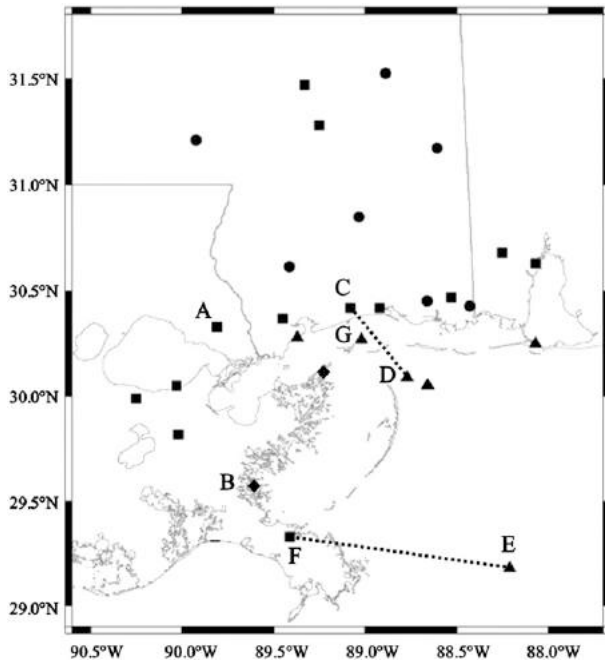


FIG. 1. Surface observing stations from which data were collected. Squares represent NOAA stations, circles represent MS RAWs, triangles represent buoys and C-MAN stations, and diamonds represent USGS National Water Information System (NWIS) stations. The denoted stations are (a) KASD, (b) 07374527, (c) KGPT, (d) buoy 42007, (e) buoy 42040, (f) KBVE, and (g) SIPM6. KASD is collocated with the KLIX WSR-88D site. The dotted lines show where ∇T calculations are performed for Table 3. Table 2 provides the station names.

(NWS) synoptic stations; U.S. Department of Agriculture (USDA) operated Remote Automated Weather Stations (RAWS); moored and Coastal-Marine Automated Network (C-MAN) buoys from the National Data Buoy Center, Louisiana State University, and the University of Southern Mississippi; and U.S. Geological Survey (USGS) tide gauges. It is worth noting that these platforms use slightly different wind-averaging procedures, with the anemometer located at somewhat different heights. The following wind-averaging and observation heights were noted: NWS stations, 1 min at 10 m; RAWS, 10 min at 6 m; moored buoys, 8 min at 5 m; the Dauphin

Island, Alabama C-MAN buoy (DPIA1), 2 min at 13.5 m; and USGS stations, instantaneous (no averaging) at 5–6 m.

The frequency and distribution of convective precipitation are examined with the level-III long-range base reflectivity product from the Weather Surveillance Radar-1988 Doppler (WSR-88D) station based in KLIX, the primary radar site for southern Mississippi, eastern Louisiana, and the adjacent waters. The level-III WSR-88D data were obtained from the National Climatic Data Center.

Surface observations and WSR-88D data were qualitatively examined to narrow the focus of the JJA 2003–05 study period to those days on which an SBC or LBC is likely to be present. Days were initially selected in which synoptic charts indicated an environment favorable for a SBC or LBC, such as a surface anticyclone positioned over the southeastern United States, resulting in a first set of “minimally synoptic” days. Wind speed values at 1200 UTC [0700 central daylight time (CDT), where CDT = UTC – 5 h] from the Slidell observing station (KASD) were observed to be less than 3.4 m s^{-1} (7.5 mi h^{-1}) for each of the initially selected days, ensuring minimal synoptic influence. From an extensive review of the level-III long-range reflectivity product from KLIX, days were removed in which an organized precipitation event or widespread airmass thunderstorm activity potentially obscures the signals of the SBC or LBC influence in the reflectivity pattern. Application of aforementioned conditions reduces the study period to 102 “sea- and/or land-breeze” (SLB) days, and improves the probability that corresponding diurnal signals of wind and precipitation indicate the presence of an SBC or LBC.

a. Surface and upper-air analysis

A monthly climatology is constructed from surface and rawinsonde data for the SLB days during 2003–05. Surface observations of temperature, wind speed, and wind direction are averaged at each hour, and the rawinsonde data are averaged every 12 h. The average hourly wind direction is obtained by

$$\overline{\text{WD}(t)} = \tan^{-1}(\bar{u}/\bar{v}) + \begin{cases} \bar{v} < 0, \\ \bar{v} \geq 0, \end{cases} \quad \begin{cases} \bar{u} \geq 0: 360 \\ 180 \end{cases}; \quad \begin{cases} \bar{u} = n^{-1} \sum_n \|u(t)\| \\ \bar{v} = n^{-1} \sum_n \|v(t)\|, \end{cases} \quad (1)$$

where t represents the hour of day and n represents the total number of SLB observations for time t . By normalizing the u and v components in each SLB observation of wind, a speed bias of the average wind direction is avoided.

To examine the variation of T (as a proxy for density), average hourly temperature gradients (∇T) are computed for two cross-shore segments along the NCGC from the following station pairs: 1) Gulfport–Biloxi International

TABLE 2. Land-based (NOAA, RAWS, USGS) and water-based stations from which observations were collected for JJA 2003–05. The last column lists the total percentage of possible hourly observations recorded during the SLB period at each observing station.

Station ID	Station name	Lat, lon	Possible SLB observations (%)
KBFM	Mobile Downtown Airport, AL	30.63°N, 88.07°W	91.1
KMOB	Mobile Regional Airport, AL	30.68°N, 88.25°W	92.7
KPQL	Pascagoula/Lott International Airport, MS	30.47°N, 88.53°W	58.3
KBIX	Biloxi/Keesler AFB, MS	30.42°N, 88.92°W	69.8
KGPT	Gulfport–Biloxi International Airport, MS	30.42°N, 89.08°W	91.2
KHBG	Hattiesburg/Chain Municipal Airport, MS	31.28°N, 89.25°W	78.9
KPIB	Laurel/Hattiesburg Pine Belt, MS	31.47°N, 89.33°W	96.0
KHSA	Bay St. Louis/Stennis International Airport, MS	30.37°N, 89.45°W	29.6
KBVE	Boothville, LA	29.33°N, 89.41°W	99.1
KASD	Slidell Airport, LA	30.35°N, 89.82°W	87.9
KNEW	New Orleans Lakefront Airport, LA	30.05°N, 90.03°W	97.7
KNBG	New Orleans/Alvin Callender Field NAS, LA	29.82°N, 90.02°W	57.6
KMSY	New Orleans International Airport, LA	29.99°N, 90.25°W	99.1
NS234	Grand Bay, Jackson County, MS	30.43°N, 88.43°W	64.3
LKKM6	Greene County, MS	31.17°N, 88.61°W	66.9
SHCM6	Mississippi Sandhill Crane, Jackson County, MS	30.43°N, 88.66°W	97.3
LSUM6	Wausau, Wayne County, MS	31.52°N, 88.89°W	65.0
BLCM6	Black Creek, Stone County, MS	30.85°N, 89.03°W	97.5
RMAM6	Marion County, MS	31.21°N, 89.92°W	98.9
07374527	Northeast Bay Gardene, LA (USGS)	29.59°N, 89.61°W	79.8
3007220891501	Mississippi Sound at Grand Pass, LA (USGS)	30.12°N, 89.25°W	72.1
DPIA1	Dauphin Island	30.25°N, 88.07°W	99.8
42040	119 km S of Dauphin Island	29.18°N, 88.21°W	92.0
42067	USM3M01 (USM)	30.04°N, 88.65°W	31.8
42007	40 km SSE of Biloxi	30.09°N, 88.77°W	97.9
SIPM6	Ship Island Pass (LSU)	30.27°N, 89.02°W	5.8
WAVM6	Waveland (NOS)	30.28°N, 89.37°W	26.3

Airport (KGPT) to buoy 42007 and 2) Boothville, Louisiana (KBVE), to buoy 42040 (see dashed lines in Fig. 1). These four stations have a denser observation history relative to other stations in the study region (Table 2). With KGPT situated on the mainland, and buoy 42007 situated relatively near the coastline, these two stations constitute the best available station pair for examining the daily evolution of surface \mathbf{VT} on SLB days for the NCGC region. The station pair of KBVE and buoy 42040 is the best available pair for assessing the \mathbf{VT} trend with any west–east-oriented SBC or LBC along the southeastern Louisiana coast. Trends of \mathbf{VT} between KGPT and 42007, and between KBVE and 42040, are compared against wind trends during case study days. Additionally, the diurnal trend of \mathbf{VT} averaged for SLB days is compared against \mathbf{VT} averaged for all days during JJA 2003–05.

b. Radar analysis

The base reflectivity product of the KLIX WSR-88D at the lowest scan angle (approximately 0.5°) is used to calculate an accumulated tabulation of 4-h rain-indicative pixels with reflectivity ≥ 30 dBZ within a circular area covered by the radar. A reflectivity value of 30 dBZ is used as a threshold for convective precipitation, consistent

with Wilson and Megenhardt (1997). An examination of radar images showed a decrease in detection of 30-dBZ values beyond 240 km. At 240 km, the radar beam height is approximately 5 km, and continues to increase in altitude away from KLIX with the curvature of the earth. Refraction and attenuation may also slightly impact the reflectivity values. Therefore, the circular area of interest is constrained with a radius of 240 km (150 mi). These accumulated tabulated values are plotted for each 4-h period of JJA to show the diurnal rainfall evolution for each month.

The circular radar region is divided into four quadrants, or sectors, to allow for a more geographically specific analysis (Fig. 2). Sector 1 covers much of coastal Louisiana and the adjacent waters of the Gulf of Mexico. Sector 2 includes the Chandeleur and Breton Sounds, as well as the Mississippi–Alabama shelf region of the Gulf of Mexico, which is enclosed by the barrier islands of Louisiana, Mississippi, and Alabama. Sector 3 primarily covers inland portions of eastern Louisiana and southwestern Mississippi, including the alluvial soil regions along the Mississippi River. Sector 4 primarily covers southeastern Mississippi and southwestern Alabama.

To quantify the rainfall coverage in each sector, the number of reflectivity pixels >30 dBZ over a 4-h period

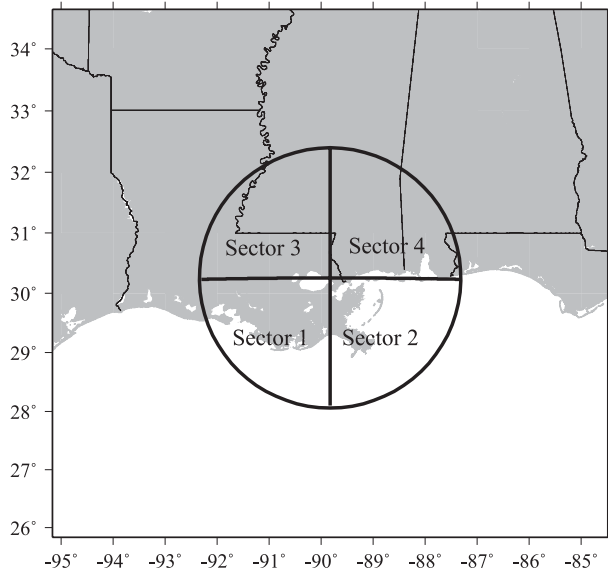


FIG. 2. The circular area, of 240-km radius, within which the KLIX WSR-88D operates. The area is divided into sectors for analysis and discussion purposes.

was computed, and then divided by all pixels in the circular radar coverage area. This quantity, defined as the areal precipitation coverage (APC), was calculated for each of six daily 4-h bins in each sector, and has a maximum value of 25% in each sector. The daily APC values are used in a multiple-regression analysis detailed later in this section, and in scatterplots. Time series plots of monthly average APCs are also used to examine the monthly average diurnal evolution patterns of the convective precipitation coverage in each sector.

c. Statistical significance tests

This study seeks to determine monthly climatology rainfall and wind patterns for SLB days. While making subjective comparisons of monthly graphical plots is a useful procedure, it is also beneficial to complement them with statistical significance tests. Furthermore, it is important to understand why these differences may exist, which can also be facilitated by graphical comparisons and significance inferences. Monthly comparisons are performed on the variables of APC: the wind speed and its vector components, u and v ; PW; and CAPE.

Except for PW, the distribution of each variable is not normally distributed. Therefore, t -test usage is invalid. A nonparametric test alternative without data distribution restrictions is the Wilcoxon rank sum test (Wilcoxon 1945; Reimann et al. 2008). The Wilcoxon approach arranges two samples in ascending (or descending) value order, a rank is assigned to each value, and the ranks are added for each sample. The significance is then assessed

(through a p value) based on the size difference between the cumulative rankings. A small p value is generally interpreted as being evidence against the null hypothesis, which is to reject the premise of no difference between the two samples. Generally, the following interpretations are used by statisticians as evidence against the null hypothesis: $0.15 > p \geq 0.05$, suggestive but inconclusive; $0.05 > p \geq 0.01$, moderately convincing; $0.01 > p \geq 0.001$, convincing; and $p < 0.001$, very convincing. These four situations are tabulated in several of the tables below as \wedge , $*$, $**$, and $***$, respectively. The upcoming discussion focuses on situations where $p < 0.01$, or time series trends with $p < 0.01$ occasionally mixed with moderately convincing p values.

d. Multiple-regression analysis

To help quantify the influences of the local thermodynamics and synoptic wind direction on the regional coastal rainfall coverage, scatterplot and multiple-regression calculations were performed for APC from each radar sector versus each of several variables corresponding to the potential for airmass thunderstorm activity. The prospective variables include CAPE, PW, 850-hPa wind direction, and KI, along with its individual components: 850-hPa T_d , 700-hPa dewpoint depression, and the 850–500-hPa lapse rate (Γ). The 0000 UTC (1900 CDT) and 1200 UTC (0700 CDT) KLIX sounding data are used in the computations.

In this study, stepwise regression with a “backward glance” selects the optimum number of most important variables using a predefined significance value (90%). An extra step is taken to ensure the proper selection of the variables, in that the initially chosen variables are examined for multicollinearity. If any of the variables are correlated with another variable by more than 0.7, the variable with less correlation to the dependent variable is removed and the regression is recalculated. In this way, only the independent variables are considered.

A normalization procedure is also applied for equal comparison between the variables. Denoting σ as the standard deviation of a variable, y as the dependent variable APC, \bar{x} as the predictor mean, and \bar{y} as the dependent variable mean, a number k of statistically significant predictors are normalized in the following regression:

$$\frac{(y - \bar{y})}{\sigma_y} = \sum_{i=1}^k c_i \frac{(x_i - \bar{x}_i)}{\sigma_i}. \quad (2)$$

The advantage of this approach is that the importance of a predictor may be assessed by comparing regression coefficients c_i between the different variables without the influence of the y intercept of each variable. In addition,

\bar{x}_i may be interpreted (to a first approximation) as a “threshold” value that distinguishes between the positive (negative) contributions of a predictor for $c_i > 0$ ($c_i < 0$).

3. Results

a. Wind speed and direction

A distinct diurnal trend of the wind can be discerned for SLB days over the area of interest, with some variation by month. In June, the wind at KGPT (representative of the Mississippi coast) veers throughout an average SLB day, being primarily northerly during the predawn hours and primarily from the south or southeast during the afternoon (Fig. 3). The wind speed at KGPT abruptly increases (decreases) soon after local sunrise (sunset). At buoy 42007, the average wind is primarily southeast, but it is more easterly and slower during the late morning. The average southeasterly wind at buoy 42040 becomes more easterly in sequence with buoy 42007, yet the wind speed at buoy 42040 is relatively steady throughout an average day, measuring between 3.4 and 4.0 m s⁻¹. During the afternoon, the winds at the coast and over the adjacent waters turn more southerly and southeasterly, respectively, indicating the influence of an SBC.

In July, general southerly flow replaces the easterly–southeasterly wind regime of June. Significance tests for zonal wind differences between June and July (Table 3) consistently range from moderately convincing to convincing for buoys 42007 and 42040 throughout the day, as well as from 0900 to 1800 CDT at KGPT. The frequent, nocturnal calm wind at KGPT from 0100 to 0800 CDT makes the significance tests difficult to apply (see Table 2 caption for more details). In addition, the average SLB day in July shows a more discrete transition from LBC to SBC. Convergence is noted between KGPT and buoy 42007 from 0200 to 0900 CDT. It is during this time that the average wind at both stations acquires a westerly component, which may indicate the presence of an LBC along the eastern Louisiana coast. As the wind speed increases at KGPT, the wind decreases and shifts to a more northerly direction at buoy 42007 from 0900 to 1200 CDT. At buoy 42040, a similar northerly wind shift takes place during 1200 to 1400 CDT. The northerly direction of the wind at buoys 42007 and 42040 suggests the influence of an LBC along the Mississippi coast, but corresponding *p* values are still high. The southerly redirection of the wind at KGPT by 1200 CDT indicates the beginning of an SBC. A cross-shore expansion of the SBC is indicated by a southerly wind turn at buoy 42007 by 1400 CDT, and at buoy 42040 by 1500 CDT. During the period of peak wind speed at KGPT (from

1200 to 1600 CDT), the wind speed at 42007 increases from a local minimum toward a maximum at 1800 CDT. Meanwhile, the wind speed at 42040 reaches a local minimum, which contrasts with the more steady wind speed in June; this difference is statistically significant from 1300 to 1800 CDT.

In August, the most prominent feature is a stronger LBC. Offshore winds occur at KGPT from 2000 to 1100 CDT, at 42007 from 0500 to 1200 CDT, and at 42040 from 0700 to 1200 CDT. The onset of the LBC offshore is 2–4 h earlier than in July. The LBC differences between July and August are significantly different for meridional winds at KGPT and 42007, as well as between June and August. As in July, the August predominant flow is southerly (note the statistically significant difference between June and August for zonal wind), and the winds at buoys 42007 and 42040 exhibit a veering pattern, with a persistent speed of 3–4 m s⁻¹ at buoy 42040. The wind has a westerly component from 0400 to 0700 CDT, and turns more northerly thereafter, in association with the LBC. The sea breeze begins at KGPT at about 1200 CDT, and the associated SBC spreads to buoy 42007 by about 1400 CDT. The wind at buoy 42040 turns more southerly later in the afternoon, and is stronger than in July, with hints of statistical significance.

It is worth noting that the inertial period, λ , for the region of study, defined by

$$\lambda = \frac{\tau}{2}; \quad \tau = \frac{2\pi}{\Omega \sin\phi}, \quad (3)$$

is approximately 24 h, where τ is the pendulum day, $\Omega = 7.292 \times 10^{-5} \text{ s}^{-1}$, and $\phi \approx 30^\circ\text{N}$. Buoys 42007 and 42040 both show a clockwise turn in July and August, which suggests inertial forcing contributes to the evolution of these wind fields (e.g., Rotunno 1983). Synoptic forcing may be overwhelming the influence of inertial forcing during the month of June. However, it is difficult to quantify the role of inertial forcing relative to the contribution of the evolving VT patterns and large-scale conditions, and so this topic will require additional future research.

For all months, the average diurnal trend of the wind speed at buoy 42007 has a phase lag of approximately 5–6 h compared to the wind speed trend at KGPT. The average wind speed at buoy 42007 reaches a relative maximum at about 0800 or 0900 CDT, a minimum at about 1200 or 1300 CDT, and then another relative maximum between 1700 and 1900 CDT. The wind speed minimum at 42007 precedes the speed maximum at KGPT by about 2 h as 42007 observes a transition to more southerly flow. The average wind speed at buoy 42040 measures no less than 2.2 m s⁻¹ and varies no more than 1.3 m s⁻¹ during an average SLB day. However, the

3-Year Wind Composite for Gulfport, 42007, 42040

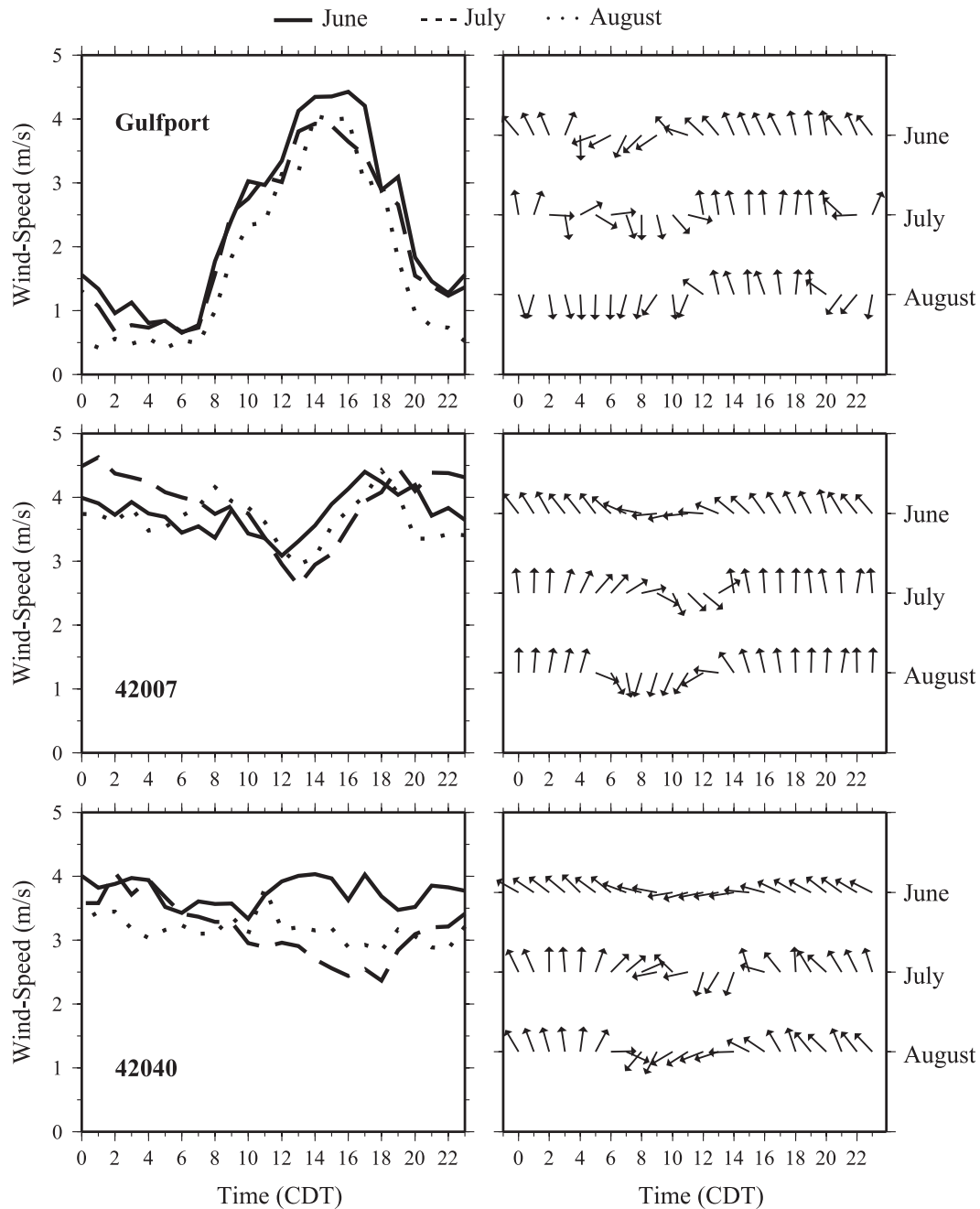


FIG. 3. Monthly SLB composites of hourly wind speed (m s^{-1}) and wind direction at (top) Gulfport, MS, (middle) buoy 42007, and (bottom) buoy 42040 for June–August; CDT = UTC – 5 h.

average wind direction at buoy 42040 follows a diurnal trend similar to buoy 42007 and at KGPT, with an apparent phase lag of up to 2 h against the average wind direction at buoy 42007.

Further analysis of the SLB period reveals other temporal and spatial patterns of the wind throughout the

study region in June (Fig. 4), July (Fig. 5), and August (Fig. 6). Onset of the sea breeze occurs by 1200 CDT for most coastal stations; the wind speed associated with the sea breeze reaches a maximum value at the coast between 1400 and 1600 CDT. Along Louisiana’s Lake Pontchartrain, a lake breeze is apparent at 1200 CDT, but

TABLE 3. Statistical significance results testing for differences in distributions between monthly winds (u , v and speed) for KGPT and buoys 42007 and 42040, using the Wilcoxon rank sum test at each hour (CDT). Here, a caret (^) denotes $0.15 > p \geq 0.05$, a single asterisk (*) denotes $0.05 > p \geq 0.01$, a double asterisk (**) denotes $0.01 > p \geq 0.001$, and a triple asterisk (***) denotes $p < 0.001$. Calm winds are not included in the calculations. The hourly sample size ranges for 0100–1300 CDT at KGPT are June, 8–19; July, 9–28; and August, 8–14. The hourly sample size ranges for 0000 and 1400–2300 CDT at KGPT are June, 19–26; July, 28–33; and August, 17–30. The hourly sample size ranges for 42007 are June, 27–28; July, 38–39; and August, 32–33. The hourly sample size ranges for 42040 are June, 27–28; July, 32–33; and August, 31–33.

Hour (CDT)	Zonal wind								
	June vs July			July vs August			June vs August		
	KGPT	42007	42040	KGPT	42007	42040	KGPT	42007	42040
0000	^	*	**					*	*
0100	^	*	*					*	*
0200	*	*	*					*	^
0300		*	**					*	*
0400	^	**	*	^				*	*
0500		**	*					^	**
0600	^	**	**					^	*
0700	^	**	**	^					**
0800	^	*	**		^				*
0900	*	*	**	**	^				*
1000	*	*	**		^				*
1100	*	***	**		*	^			
1200	*	***	***		*	*			^
1300	**	***	***		*	^		^	^
1400	*	**	***		^	*		*	^
1500	^	**	***			*	^	*	*
1600	*	**	***				^	*	**
1700	**	**	***				^	*	**
1800	**	**	***				^	^	**
1900		^	*					*	*
2000			*						**
2100		^	^					*	*
2200		**	*					*	*
2300	*	**	**			^		**	^

Hour (CDT)	Meridional wind								
	June vs July			July vs August			June vs August		
	KGPT	42007	42040	KGPT	42007	42040	KGPT	42007	42040
0000				*	^		*		
0100				**	*		*	^	
0200				**	**		*	^	
0300				^	*		*		
0400				**	*		^	^	
0500				*	**	^	*	*	
0600				**	*	^	^	**	^
0700				**	***	^	*	**	
0800				^	**		*	**	
0900					**		^	**	^
1000	^				**		*	**	
1100				*	*	^	*	**	
1200				^	^		^	*	
1300								^	
1400	^								
1500							*		
1600	^								
1700	^				^				
1800	^		^				^		
1900							^		

TABLE 3. (Continued)

Hour (CDT)	Meridional wind								
	June vs July			July vs August			June vs August		
	KGPT	42007	42040	KGPT	42007	42040	KGPT	42007	42040
2000			*						*
2100				^	^		^		^
2200					*		^	^	
2300					*		^		

Hour (CDT)	Total wind speed								
	June vs July			July vs August			June vs August		
	KGPT	42007	42040	KGPT	42007	42040	KGPT	42007	42040
0000					*				
0100		^		^	*				
0200	^	^			*	^			
0300					^				^
0400					*	^			^
0500						^			
0600	^								
0700	^			*					*
0800									
0900									
1000				*			*		
1100			^						
1200			^						
1300		^	*					^	^
1400			**					^	*
1500		*	**			^		^	^
1600	**	*	*				*	^	^
1700	**		***						**
1800			**						*
1900			^				**		
2000									
2100		^			*				^
2200					*	^			*
2300		^			*				

is later enveloped by a larger and more dominant SBC spanning the marshlands of southeastern Louisiana. During the nighttime, the larger-scale sea breeze along the lakeshore transitions into a southerly land breeze. The north-south-oriented SBC can readily expand across the flat terrain of southeastern Louisiana. At Bay Gardene, Louisiana, a west-east-oriented SBC initially develops by 1200 CDT in each of June, July, and August, and is later enveloped by the larger north-south-oriented SBC by 1600 CDT. The average wind at this location acquires a westerly component by 0400 CDT of July and August, indicative of a west-east-oriented LBC. Note that a westerly wind component is evident at buoys 42007 and 42040—downwind of Bay Gardene—after 0400 CDT and before 0800 CDT (Fig. 3). In June, the average wind at Bay Gardene conforms to the predominant southeasterly flow over the Gulf waters, and suppresses any possible

LBCs over eastern Louisiana. Hence, in the absence of a southeasterly wind regime in July and August, inertial forcing may help to initiate or enhance an LBC over eastern Louisiana and adjacent waters after the north-south-oriented SBC dissipates and before the Mississippi LBC becomes dominant.

b. Cross-shore temperature gradient

A summary of average VT values calculated between the selected cross-shore station pairs is provided in Table 4. The average daily minimum (maximum) VT values between KBVE and buoy 42040 are about 19%–23% (28%) of the values between KGPT and buoy 42007; much of the difference is due to the greater relative distance between KBVE and buoy 42040.

A cross-shore VT associated with an SBC or an LBC is ideally measured between equidistant points on each

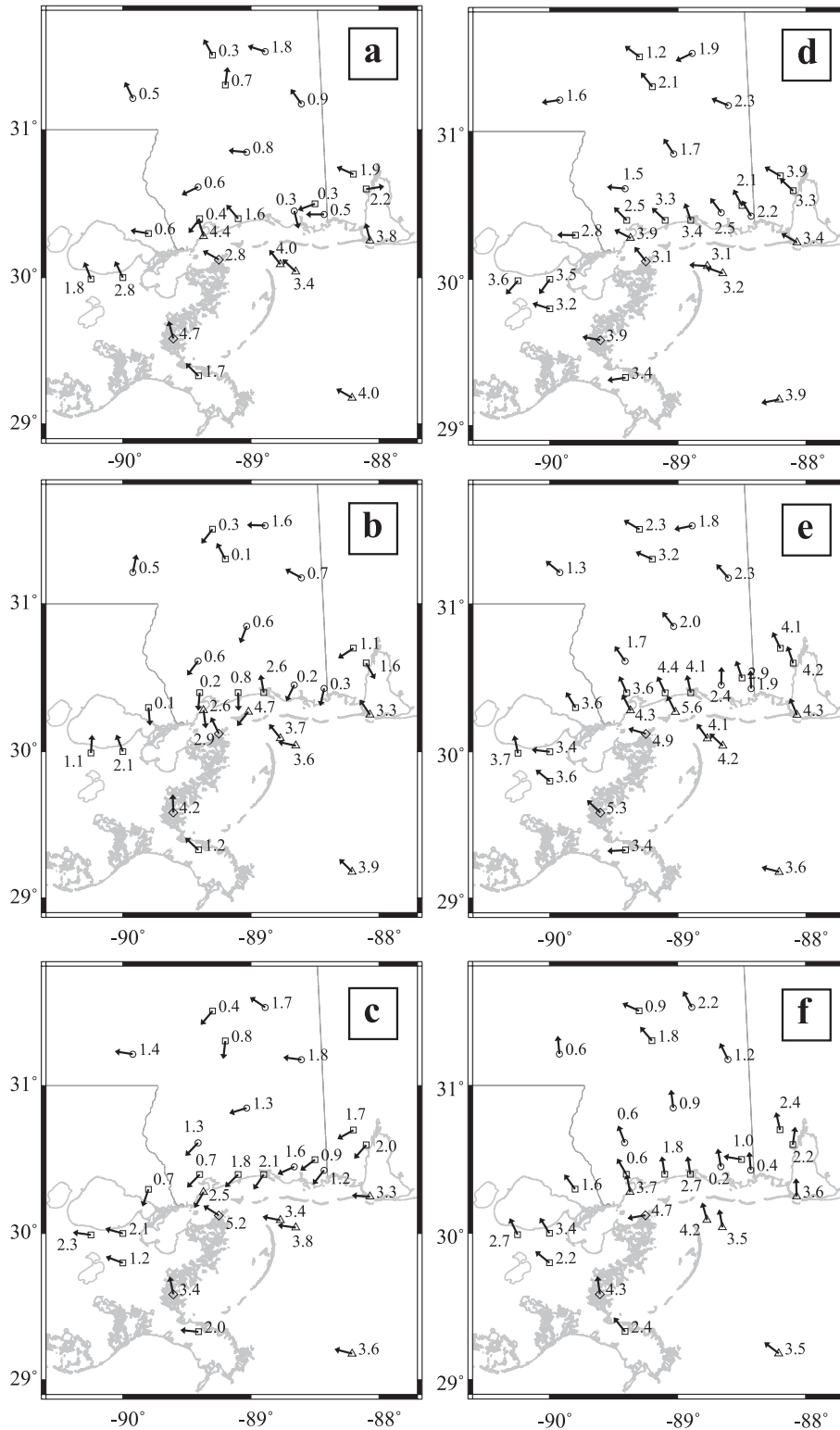


FIG. 4. June SLB composite of hourly wind direction and wind speed (m s^{-1}) for all stations in the study region for (a) 0000, (b) 0400, (c) 0800, (d) 1200, (e) 1600, and (f) 2000 CDT. Wind direction is represented by vectors, and wind speed is plotted as a number in units of m s^{-1} .

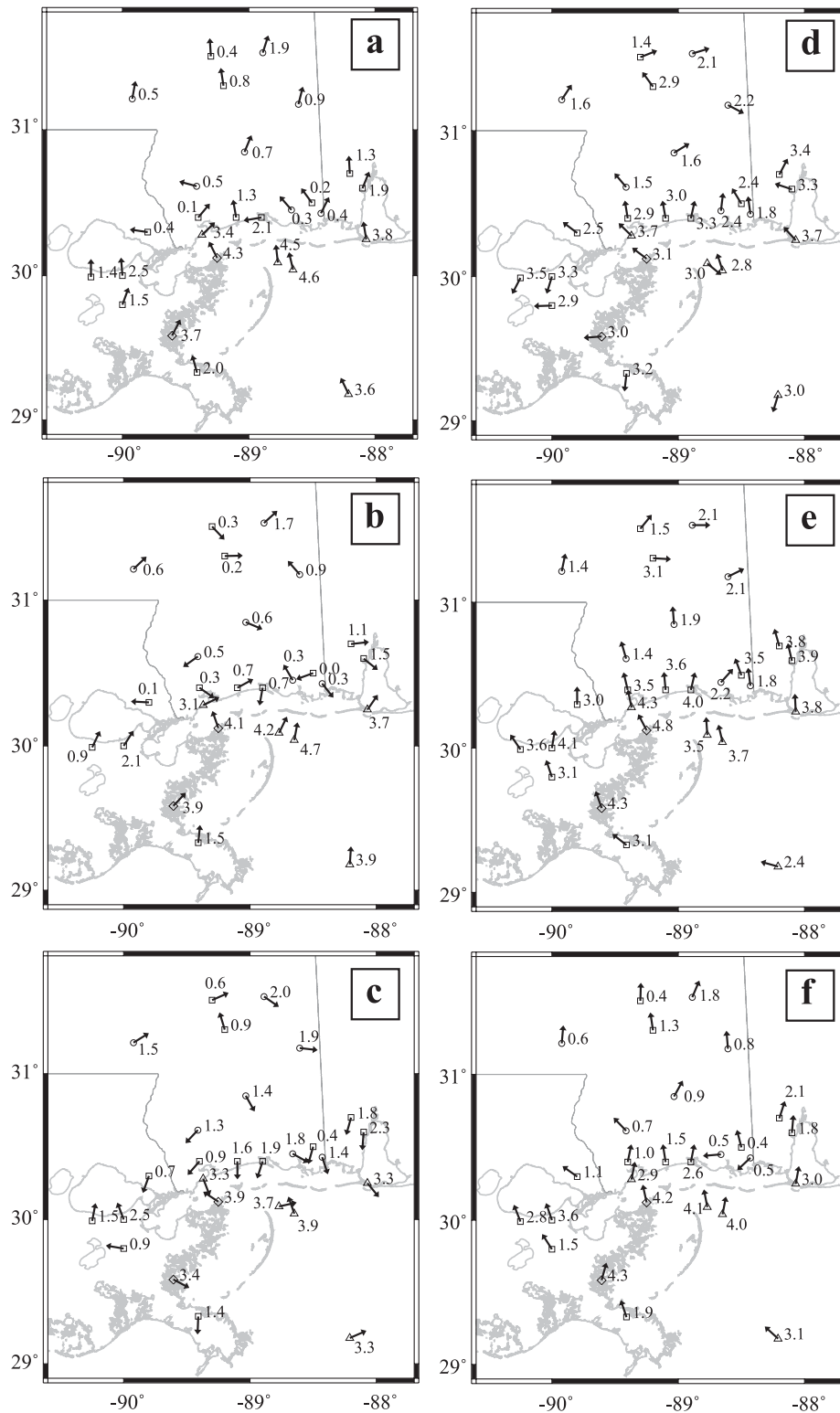


FIG. 5. As in Fig. 4, but for July.

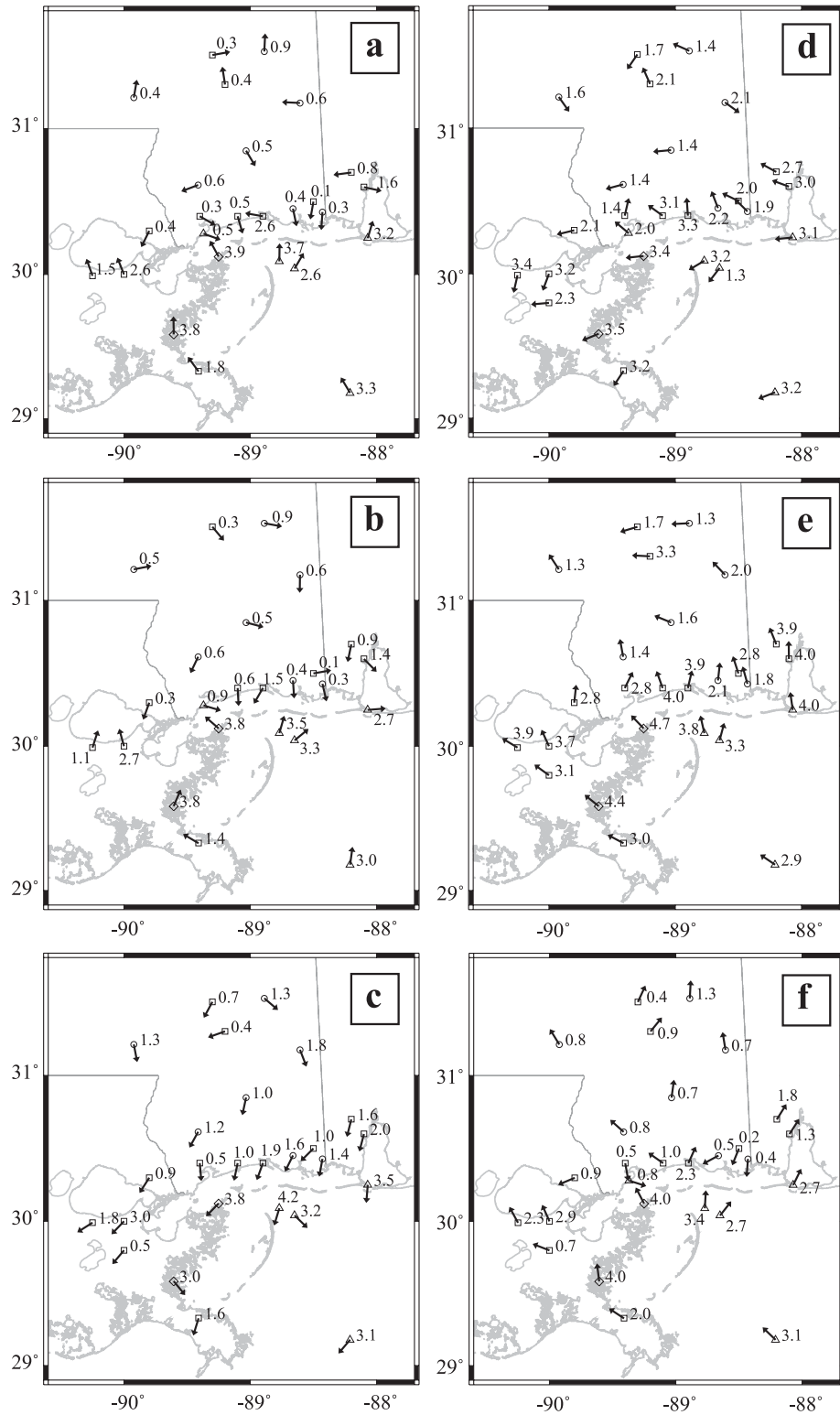


FIG. 6. As in Fig. 4, but for August.

TABLE 4. Average daily minimum and maximum ∇T (K km^{-1}) between land-based stations and buoys for each of June, July, and August during the SLB days of 2003–05. See Fig. 1 for cross-shore locations. The original gradient is calculated with the true distance between stations. The revised gradient is calculated with the total distance equal to twice the distance of the land-based station to the shoreline. Hourly sample size ranges for KGPT vs 42007 are June, 26–28; July, 37–39; and August, 31–33. Hourly sample size ranges for KBVE vs 42040 are June, 26–28; July, 38–39; and August, 31–32.

Month	KGPT vs buoy 42007			KBVE vs buoy 42040		
	Time (CDT)	Original gradient	Revised gradient	Time (CDT)	Original gradient	Revised gradient
June, min	0600	-7.66×10^{-5}	-4.52×10^{-4}	0300	-1.74×10^{-5}	-2.57×10^{-4}
June, max	1400	6.89×10^{-5}	4.07×10^{-4}	1500	1.93×10^{-5}	2.84×10^{-4}
July, min	0600	-7.33×10^{-5}	-4.33×10^{-4}	0500	-1.71×10^{-5}	-2.51×10^{-4}
July, max	1200	5.96×10^{-5}	3.52×10^{-4}	1200	1.68×10^{-5}	2.48×10^{-4}
August, min	0600	-9.43×10^{-5}	-5.56×10^{-4}	0300	-1.77×10^{-5}	-2.61×10^{-4}
August, max	1400	5.57×10^{-5}	3.29×10^{-4}	1100	1.54×10^{-5}	2.26×10^{-4}

side of the shoreline. In a weak synoptic regime, as is often observed during the summertime, the air temperature field over the adjacent Gulf waters is homogeneous relative to the temperature field over land. The offshore observing station nearest to KGPT, SIPM6 (see Table 2 for a listing of the stations used in this study), is located 16 km to the southeast, but only had observations in August 2004, June 2005, and July 2005 (see Fig. 1). The next nearest offshore station, buoy 42007, is located 47 km southeast of KGPT. The average hourly range of air temperature differences from SIPM6 to buoy 42007 is from -0.7 to 0.5 K (Fig. 7), which is much less than the difference ranges found from KGPT to SIPM6 (-3.0 to 2.5 K), and from KGPT to buoy 42007 (-3.5 to 3.0 K). The small differences between SIPM6 and 42007 suggest weak ∇T offshore. With few observations to draw from, SIPM6 is discounted from our cross-shore ∇T analysis, and we rely instead on the KGPT–42007 gradient to assess the intensity of the SBC and LBC along the Mississippi coast. We must draw from limited data to compare circulation intensities along the eastern Louisiana coast.

KGPT and KBVE are approximately 4 km from their respective nearest points along the Gulf shoreline. If we assume that the air temperature 4 km offshore of these shoreline points, or 8 km from KGPT and KBVE, is equal to the air temperatures observed by the nearest reliable buoy stations (42007 and 42040, respectively), then the resulting ∇T calculated along these 8-km cross-shore segments may better depict the intensity of the local SBC and LBC. The average daily minimum (maximum) values of ∇T along the 8-km cross-shore segment including KBVE are 47%–58% (69%–70%) of the ∇T values calculated along the cross-shore segment including KGPT. As pointed out by Smith et al. (2005), southeastern Louisiana is composed of flat marshland surrounded by Gulf waters that would tend to suppress the cross-shore ∇T . The more forested Mississippi coast slopes

more steeply inland and is subject to greater temperature variability, which explains the difference of the spatially adjusted ∇T extremes calculated here. This suggests that an SBC or LBC along the Mississippi coast will tend to be stronger than an SBC or LBC along the southeastern Louisiana coast.

It stands to reason that, if an SBC and LBC are driven by a greater cross-shore ∇T , then the average monthly ∇T across the Mississippi coastline should be greater for SLB days, compared against all days, of a given month. However, the average ∇T across the Mississippi coastline is found to be amplified only for SLB days in June relative to all days during June 2003–05 (Fig. 8a). Compared against all days during July 2003–05, the ∇T across the Mississippi coastline is generally weaker (stronger) in the morning (afternoon) for SLB days in July (Fig. 8b). The weaker morning gradient observed with SLB days compared against all days of July could be a reflection of

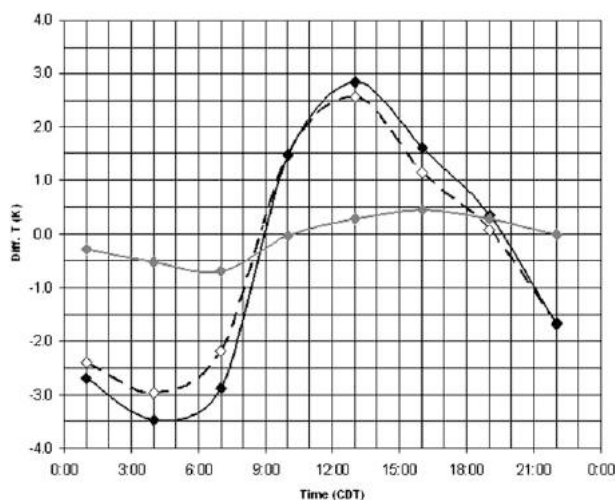


FIG. 7. Average difference in the air temperature (K) between KGPT and buoy 42007 (black solid line), KGPT and SIPM6 (dashed line), and SIPM6 and buoy 42007 (gray line).

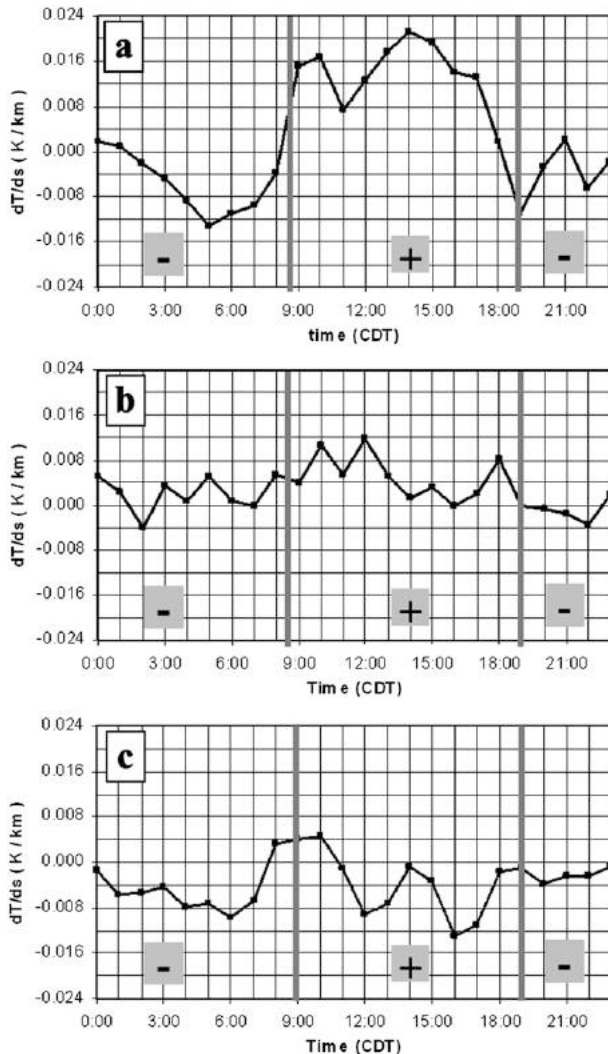


FIG. 8. Differences in the KGPT vs buoy 42007 air temperature gradient ($K\ km^{-1}$) between SLB days and all days during (a) June, (b) July, and (c) August. Gray lines indicate the approximate time when the average gradient value is zero for SLB days, with a minus sign (-) indicating the average period of negative temperature gradient and a plus sign (+) indicating the average period of positive temperature gradient.

cooler morning temperatures at KGPT during the synoptically active (non-SLB) days, in addition to an overall less-energetic LBC signal. Conversely, the SLB cross-shore ∇T is stronger (weaker) during the morning (afternoon) than the average gradient for all days during August 2003–05 (Fig. 8c). Here, a weaker SBC signal may be supplemented by higher afternoon temperatures at KGPT during non-SLB days. The monthly variations of cross-shore ∇T likely have implications for the average SBC–LBC intensity and, as will be shown later, the average daily distribution of convective precipitation for each month.

c. Rainfall patterns

While scattered thunderstorms are possible anywhere within the KLIX WSR-88D scan area on most any day, the climatology prepared here clearly associates the sea-land breeze to areal coverage of precipitation, with a common diurnal pattern noted for SLB days during JJA 2003–05 (Figs. 9–11). During the local nighttime hours, specifically between 2300 and 0700 CDT, precipitation is most prevalent offshore of the Louisiana coast, with a focus near either Atchafalaya Bay or Terrebonne Bay (location shown in Fig. 9a). After sunrise, the focus of the precipitation shifts eastward to the Mississippi–Alabama Shelf region. By 1100 CDT, precipitation is observed over coastal regions, with particular focus over southern Louisiana and near Mobile Bay (location shown in Fig. 9a). Local afternoon precipitation is widespread throughout the inland areas covered by the KLIX WSR-88D, while precipitation is at a minimum offshore. The focus of convection along the coast during the local afternoon, and over the adjacent waters during the local morning, agrees well with the diurnal pattern of lightning strikes previously found for this region during the period of May–September (Smith et al. 2005).

Monthly variations exist, however, especially in the eastern sectors of the study area. Time series plots of monthly mean APC in the eastern sectors are shown in Fig. 12 to facilitate this study, along with statistical significance testing for difference in distributions between monthly APCs in sectors 2 and 4 (Table 5). Sector 4 (coastal Mississippi) shows statistically significant less rain coverage in June than July. The August mean APC is similar to the July mean APC (no significant difference) in this sector, although Fig. 12 shows less precipitation coverage for August. Table 5 also shows that the mean nocturnal APC for June is less than for July and August at moderately convincing to convincing levels.

Sector 2 (offshore Mississippi) also shows June with the lowest mean APC. However, August shows a much larger mean APC from 0300 to 1500 CDT relative to the other months. The difference between August and June is convincingly significant during this period. Moderately convincing differences exist between July and August for 0300–1100 CDT. In the afternoon period when precipitation decreases offshore, the rainfall coverage is greater in July than in June with p levels being moderately significant to significant.

These monthly distinctions result from the different wind patterns discussed in section 3a, as well as from thermodynamic variations. Summer airmass thunderstorms require the presence of instability and a moist middle troposphere to prevent their decay from entrainment. CAPE

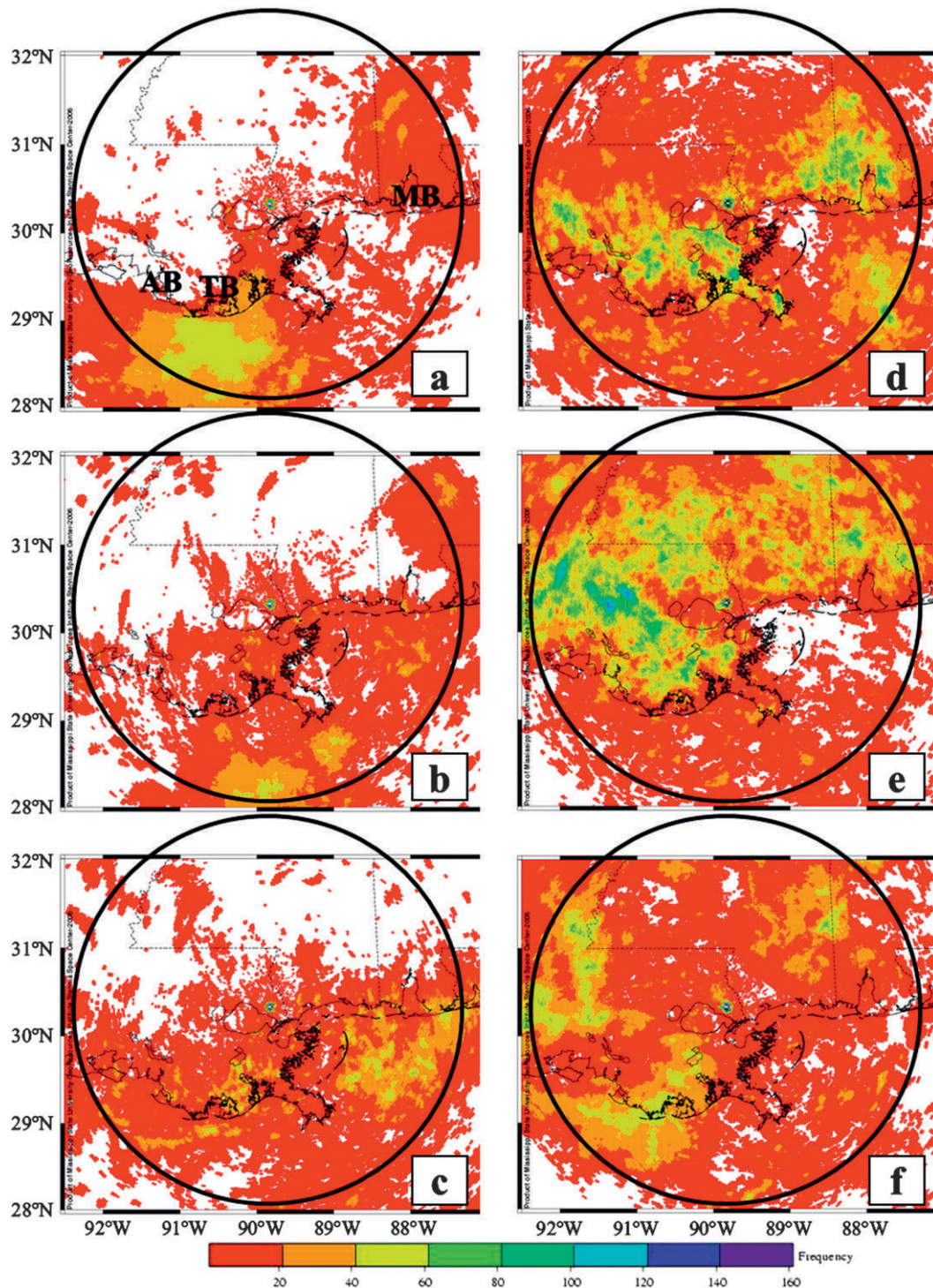


FIG. 9. June 2003–05 SLB composite frequency of rain pixels with reflectivity ≥ 30 dBZ scanned by the KLIX WSR-88D during the periods of (a) 2300–0300, (b) 0300–0700, (c) 0700–1100, (d) 1100–1500, (e) 1500–1900, and (f) 1900–2300 CDT. Frequency is shaded for every 20 counts. Circles represent the radar scan area with a radius of 240 km. The labels AB, TB, and MB in (a) refer to Atchafalaya Bay, Terrebonne Bay, and Mobile Bay, respectively.

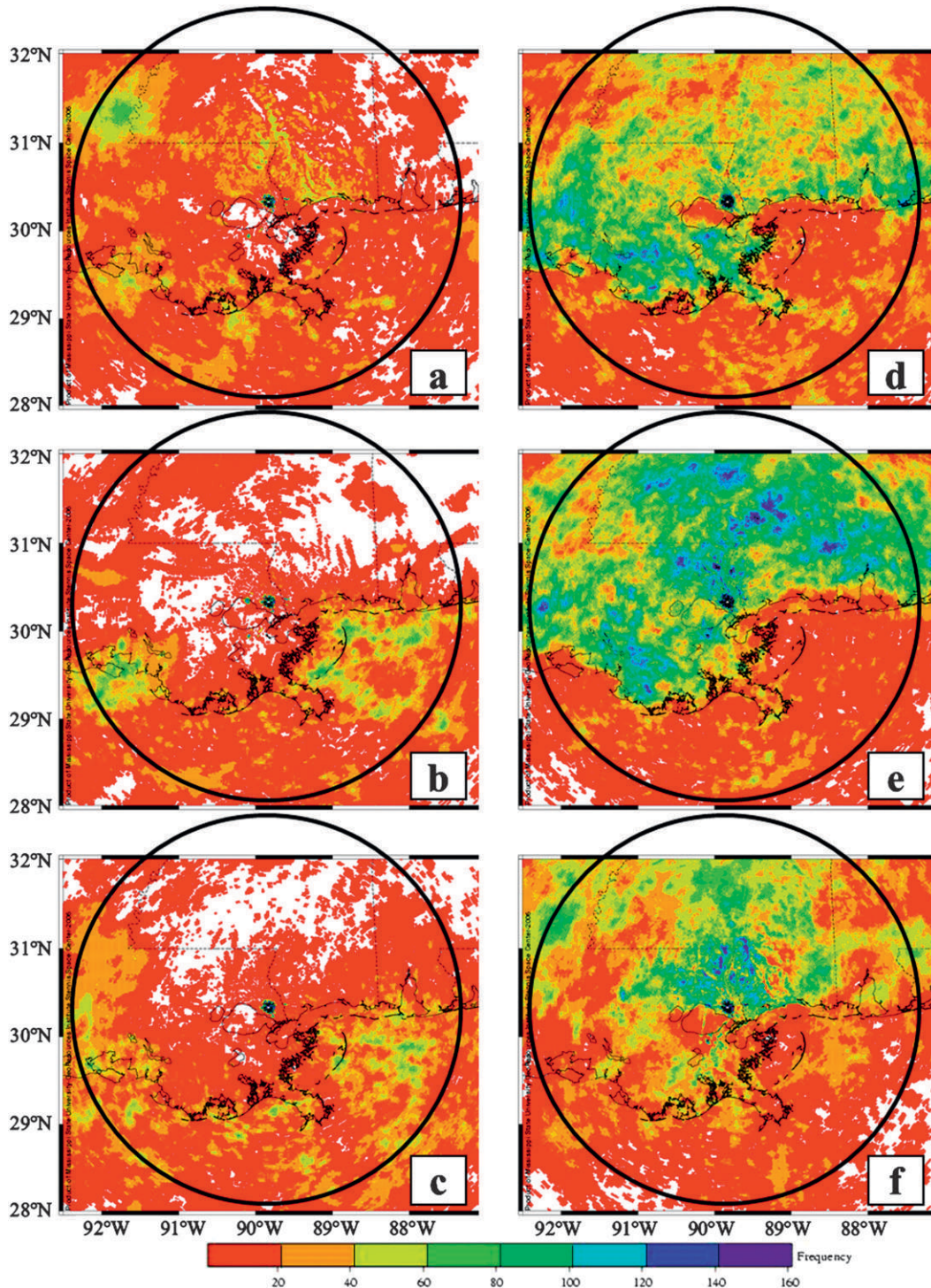


FIG. 10. As in Fig. 9, but for July.

and PW quantify these conditions. Figures 13 and 14 show monthly histograms of the PW and CAPE, respectively, and monthly significant differences are shown in Table 6. The mean June PW totals are 42 and 39 mm for

1900 and 0700 CDT, respectively. For both July and August at both time periods, the mean PW is 46 mm. It is obvious that the mean PW distribution has shifted to greater values in July and August compared to June.

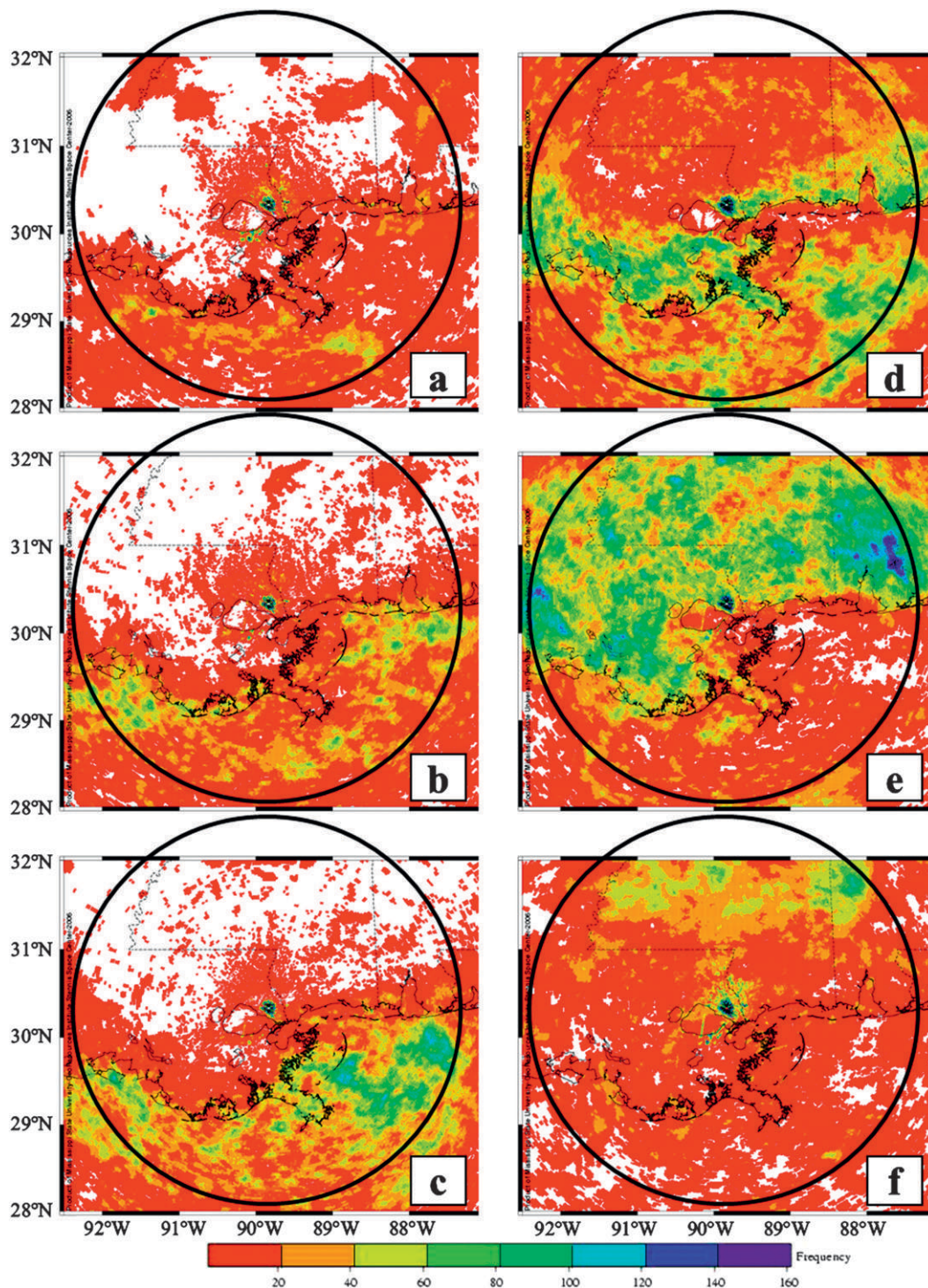


FIG. 11. As in Fig. 9, but for August.

The significance level features very convincing p levels at 0700 CDT, and moderately convincing to convincing differences at 1900 CDT for June versus July and June versus August; no significance difference is noted

between July and August. The reason for the PW increase in the mid- and late summer requires more research, but we postulate that June is a transition month in which drier air exists over land before the Bermuda

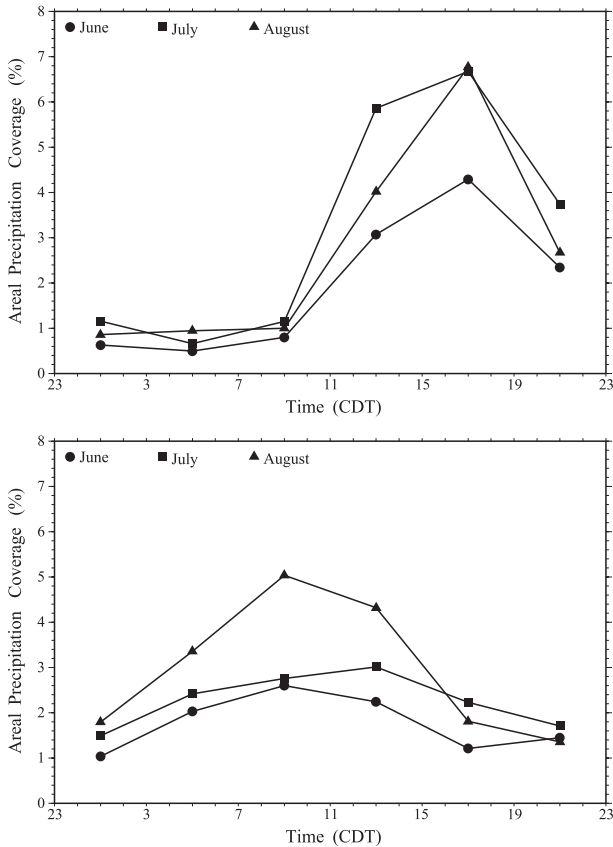


FIG. 12. The 4-hourly APC averaged over the period of 2003–05 for each month in (top) sector 4 representing inland coastal MS and (bottom) sector 2 representing offshore MS.

high transports more moisture into the region. If the PW increases as the summer progresses, naturally the CAPE will also increase. The mean CAPE values at 1900 CDT during June, July, and August are 1235, 1667, and 1736 J kg⁻¹, respectively, and 194, 318, and 308 J kg⁻¹ at 0700 CDT. However, these CAPE differences are only moderately significant, and the histograms visually do not show clear variations.

Based on these results, it is reasonable to conclude that rainfall coverage increases in July and August along

the Mississippi coast are due to more moist atmospheric layers and, to a lesser extent, additional instability. These thermodynamic variables will be further examined by a multiple-regression analysis in the next subsection. However, the increase in APC offshore of Mississippi in July and August results from additional factors. PW variability certainly contributes to offshore rain coverage, since June overall has less APC. The increase of APC in July and August is also related to the setup of the LBCs discussed in section 3a. As had been previously suggested by Smith et al. (2005), converging land breezes from Mississippi and eastern Louisiana provide convergence and additional lift for convection, which explains the increase in the APC values in those months. The LBC along the Mississippi coast tends to be stronger in August, and may explain the increase in APC during August compared to July.

d. Statistical associations with APC

Generally, only weak multiple-regression relationships were found in this study. This accentuates the importance of local dynamics and VT daily variations for SBC- and LBC-related convection. The regression is also limited by sounding data availability from solely one location (KLIX) at just two times (1900 and 0700 CDT). Nevertheless, some information was gleaned from the analysis.

The 1900 CDT sounding data were correlated to 1900–2300, 2300–0300, and 0300–0700 CDT APC data in sectors 1–4; likewise, 0700 CDT sounding data were correlated to the next three 4-h APC data periods. The analyses allowed for 24 multiple-regression runs. PW and CAPE exhibited the overall best relationships to convective activity along the Louisiana–Mississippi coast, while other variables had weaker associations or were not significant. Additionally, within some 4-h periods, little to no convection occurred, and therefore no meaningful variable correlation was produced.

Because the data sample was small for multiple-regression usage, the significance level was set at 70% so

TABLE 5. Statistical significance testing for differences in distributions results between monthly APC for sectors 2 and 4 using the Wilcoxon rank sum test at each 4-h bin (CDT). Symbols are as in Table 3. Sample size ranges are sector 2, 25–28 (June); sector 2, 40–41 (July); sector 2, 33 (August); sector 4, 25–28 (June); sector 4, 40–41 (July); and sector 4, 33 (August).

Hour (CDT)	June vs July		July vs August		June vs August	
	Sector 2	Sector 4	Sector 2	Sector 4	Sector 2	Sector 4
2300–0300	^	*			*	**
0300–0700	^	^	*	^	**	**
0700–1100		^	*		**	^
1100–1500	*	**		^	**	
1500–1900	**	*			**	^
1900–2300	^	^				

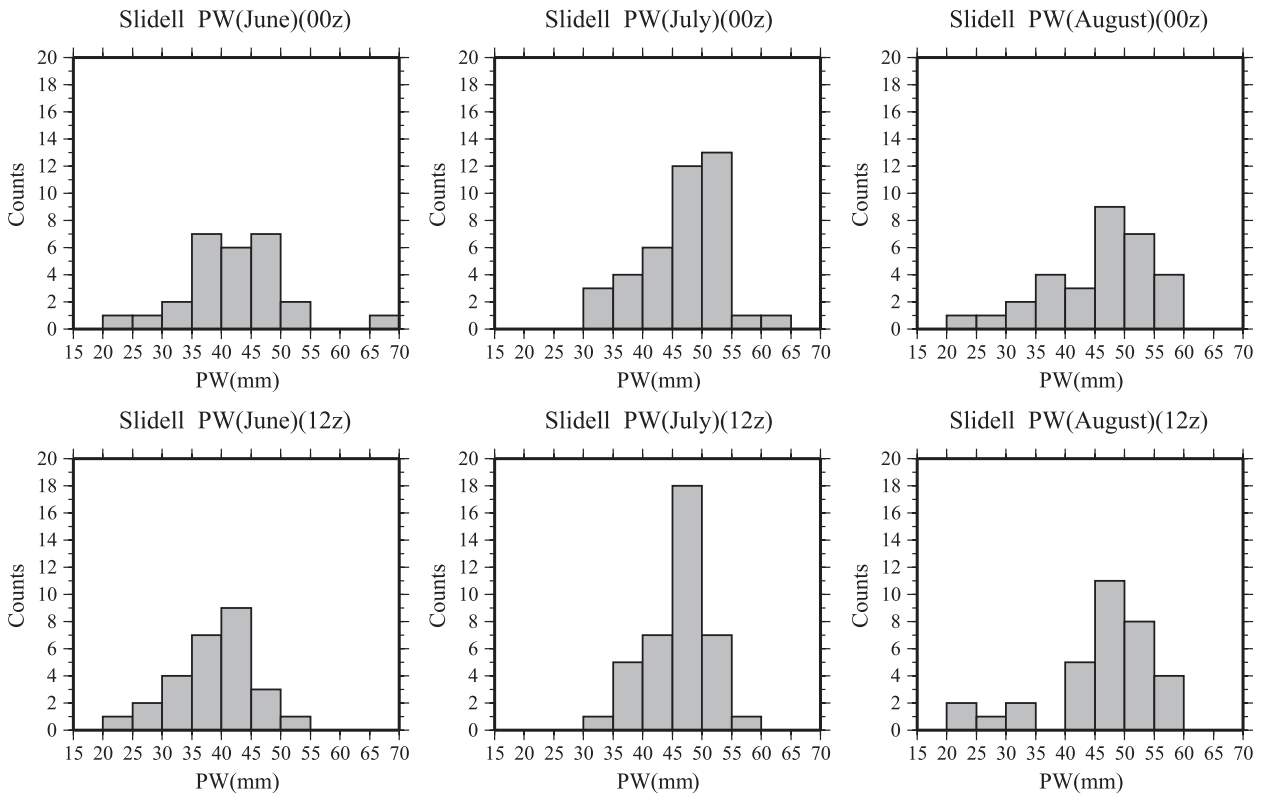


FIG. 13. Histograms of PW (mm) at KLIX for June–August for days with no synoptic influences during 2003–05. (top) The 0000 UTC (1900 CDT) soundings with sample sizes of 27, 40, and 31, respectively. (bottom) The 1200 UTC (0700 CDT) soundings with sample sizes of 27, 39, and 33, respectively.

that weakly correlated variables could be noted and to assist the backward glance component of the stepwise regression. All chosen variables of at least 90% significance were tallied. PW was selected the most (17 times), followed by CAPE (11 times), 850-hPa T_d (5 times), 850–500-hPa Γ (4 times), and 850-hPa wind direction (3 times). Often, PW and CAPE were chosen together in the multiple-regression analysis, while other variables were intermittently included.

KI was seldom chosen from the multiple-regression analysis and was rarely greater than the 90% significance level when selected, which is somewhat surprising since KI is widely perceived to be a good indicator of airmass thunderstorm coverage. The 700-hPa dewpoint depression was found to be strongly correlated to KI and, therefore, was excluded from the analysis by the multicollinearity filtering process. The relationship of KI to the probability of precipitation (PoP) and APC is examined in the appendix.

A typical multiple-regression result is provided in Table 7, which focuses on the eastern sectors of the radar coverage. Sectors 1 and 3 yielded somewhat similar results, but those results are less distinctive since much of

this region is over land. Table 7 shows results for offshore morning convection associated with the LBC, and afternoon inland convection associated with the SBC. These are periods of peak convective activity along the density currents and are the times of most importance. In both cases, PW has the largest normalized regression coefficient, followed by CAPE; both are significant at the 99% level. The 850-hPa T_d appears in each case with 90% significance and with $c_i < 0$. The correlation between 850-hPa T_d and PW is 0.57 in both cases, and the negative c_i reflects some multicollinearity between these two variables. The negative coefficient for the 850–500-hPa Γ corresponding to the offshore convection from 0700 to 1100 CDT suggests that the presence of an inland boundary layer lid from an inversion or slightly positive Γ may be conducive to offshore convection. It is unknown if its role is to inhibit onshore convection, or if a lid is also present offshore that delays convection until sufficient lift by land-breeze interactions can overcome the negative buoyancy.

Little convection occurs over inland (offshore) Mississippi from 0700 to 1100 (1500 to 1900) CDT since the lifting mechanism is usually missing. Therefore, the

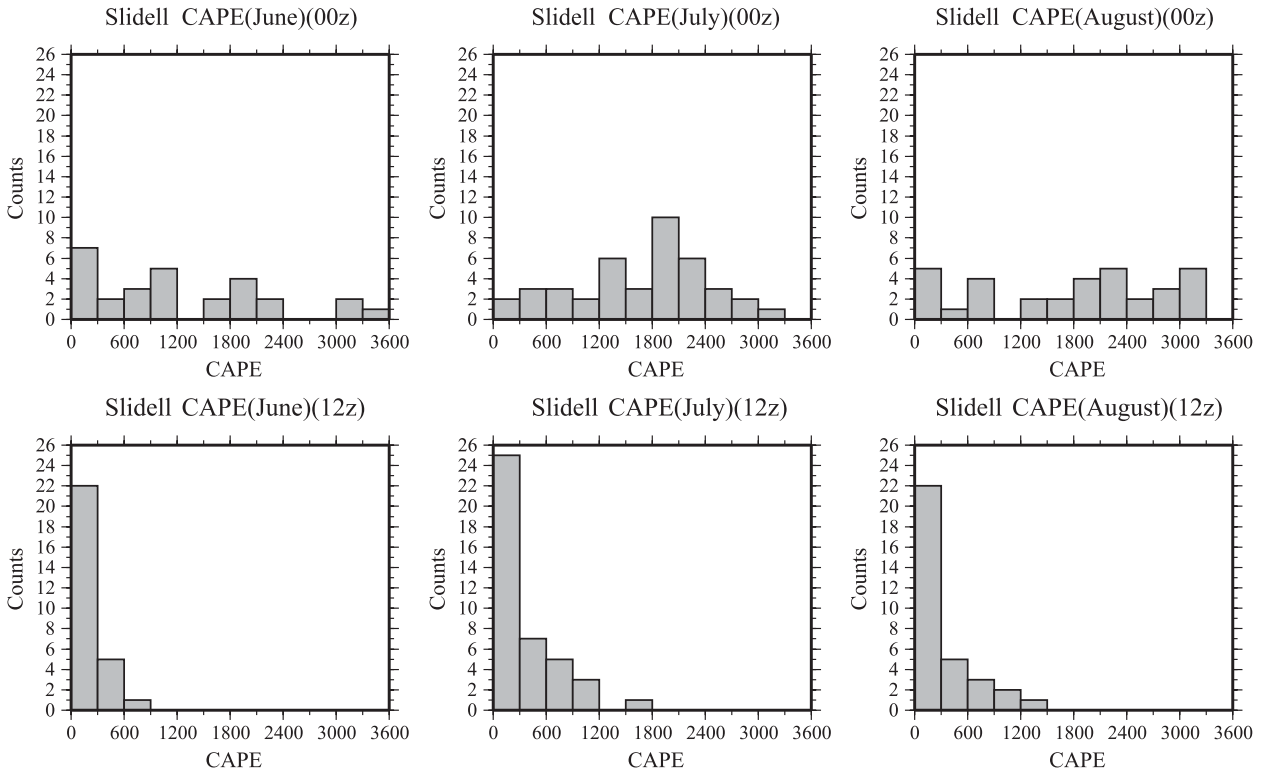


FIG. 14. As in Fig. 13, but for CAPE. Sample sizes are 28, 41, and 33, respectively, for both 0000 and 1200 UTC (1900 and 0700 CDT).

variance explained by sounding data will be small. However, the 850-hPa wind direction is determined to be a significant variable in the “dry,” or inactive, sectors during the times of the SBC and LBC with $c_i > 0$. With the mean 850-hPa wind direction calculated as 185° , a westerly (easterly) wind component weakly corresponds to the development (suppression) of convection in the inactive sectors. Scatterplots of APC versus 850-hPa wind direction for 0700 to 1100 CDT and for 2000 to 0000 CDT in the inactive sectors (not shown) indicate a larger number of high-APC values for south-southwesterly to westerly winds. In these instances, we hypothesize that the Bermuda high is positioned farther eastward from the study area, allowing convection to develop.

The multiple-regression analysis indicates that vertical columns with abundant moisture are more conducive for greater APC, given the presence of CAPE and low-level convergence associated with an SBF or an LBF. The large unexplained variance in convectively active sectors also indicates the importance of low-level dynamics fields, daily variations in SBCs and LBCs, and unresolved thermodynamic spatial-temporal variations. Nevertheless, PW does provide some information about APC potential (Fig. 15) in the convectively active and inactive sectors presented in Table 7. The active sectors show a wide distribution of APC versus PW with a weak

linear trend. More noteworthy, however, is that the larger values of PW follow a linearly increasing trend for APC in the active sectors. From this trend, a maximum potential value of APC can be discerned for a given value of PW, roughly analogous to the trend of maximum potential intensity (MPI) of a tropical cyclone against the sea surface temperature (Evans 1993; DeMaria and Kaplan 1994b). A potential APC value as a function of PW in SLB

TABLE 6. Statistical significance results between the monthly PW and CAPE for 0000 UTC (1900 CDT) and 1200 UTC (0700 CDT) using the Wilcoxon rank sum test. Symbols are as in Table 3. Sample sizes for CAPE are June, 28; July, 41; and August, 33. PW are generally 1–2 less due to missing upper-tropospheric dewpoint data.

	PW	
	0700	1900
June vs July	***	**
June vs August	***	*
July vs August	—	—
	CAPE	
	0700	1900
June vs July	*	*
June vs August	*	^
July vs August	—	—

TABLE 7. Variables chosen from a stepwise multiple-regression routine for dependent variable APC during the SLB days of 2003–05 at sector 2 (inland MS, northeast quadrant of radar coverage) and at sector 4 (offshore MS, southeast quadrant). The left column represents the morning period when the offshore convection associated with the land breeze occurs. The right column represents the afternoon period when the onshore convection associated with the sea breeze occurs. Here, R^2 is the multiple coefficient of determination (explained multiple-regression variance), and c is the normalized regression coefficient [see Eq. (2)]. Sample sizes are 97 for 0700 to 1100 CDT and 99 for 1500–1900 CDT.

	0700–1100 CDT (land-breeze convection)	1500–1900 CDT (sea-breeze convection)
Sector 4	$R^2 = 4\%$ 850-hPa wind direction* ($c = 0.19$)	$R^2 = 29\%$ PW** ($c = 0.48$) CAPE** ($c = 0.26$) 850-hPa T_d * ($c = -0.18$)
Sector 2	$R^2 = 19\%$ PW** ($c = 0.37$) CAPE** ($c = 0.29$) 850–500 hPa Γ^* ($c = -0.21$) 850-hPa T_d ($c = -0.16$)	$R^2 = 6\%$ PW* ($c = 0.23$) 850-hPa wind direction ($c = 0.11$)

* Variables significant at the 90% level ($p < 0.1$).

** Variables significant at the 99% level ($p < 0.01$).

situations could be used in a multiple-regression prediction scheme similar to the way MPI is used by DeMaria and Kaplan (1994a).

It is no surprise that CAPE is a determining factor for APC, but its contribution is apparently secondary for coastal convective development (Fig. 16). CAPE

typically only explains 10%–13% of the variance (r^2) of APC, yet CAPE is not correlated to PW ($r^2 \approx 7\%$ – 8%). Hence, CAPE and PW each contribute to LBC and SBC convection. More research is needed to understand the role of these factors and others in the development of summertime convective at the coast.

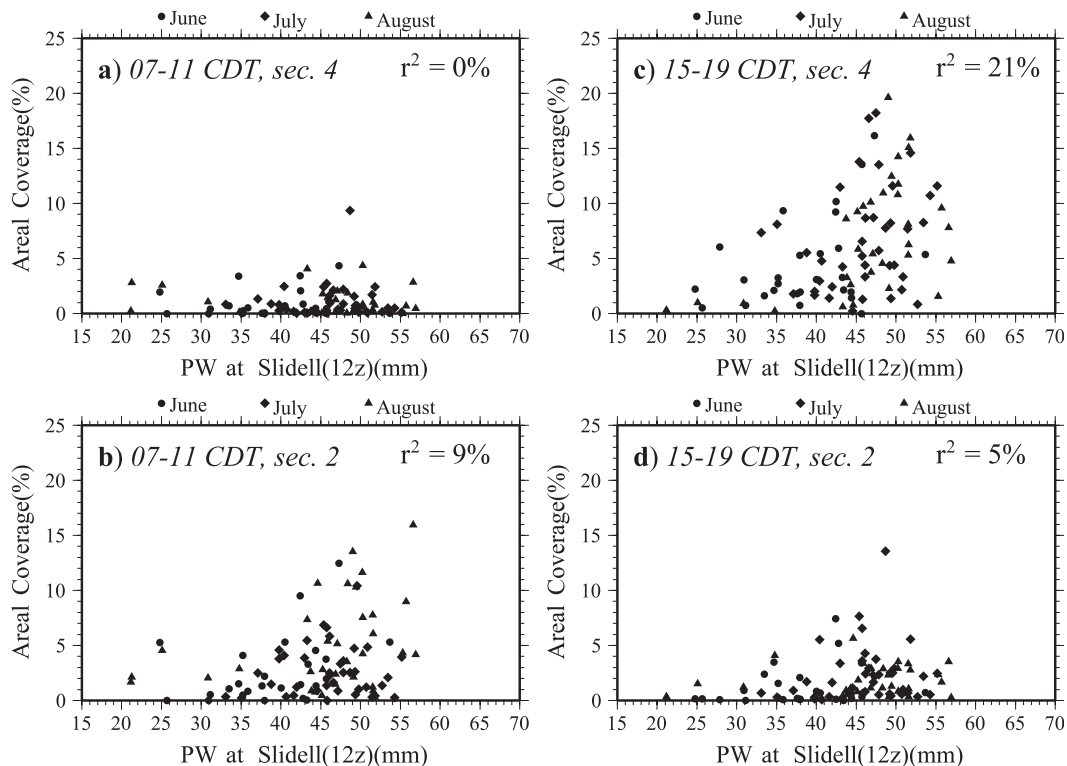


FIG. 15. SLB-period 2003–05 scatterplots of 1200 UTC (0700 CDT) PW at KLIX vs APC for 0700–1100 CDT for (a) the inland MS coast (sector 4) and (b) the offshore MS coast (sector 2), and at 1500–1900 CDT for sectors (c) 4 and (d) 2. Values of r^2 represent the variance between PW and APC.

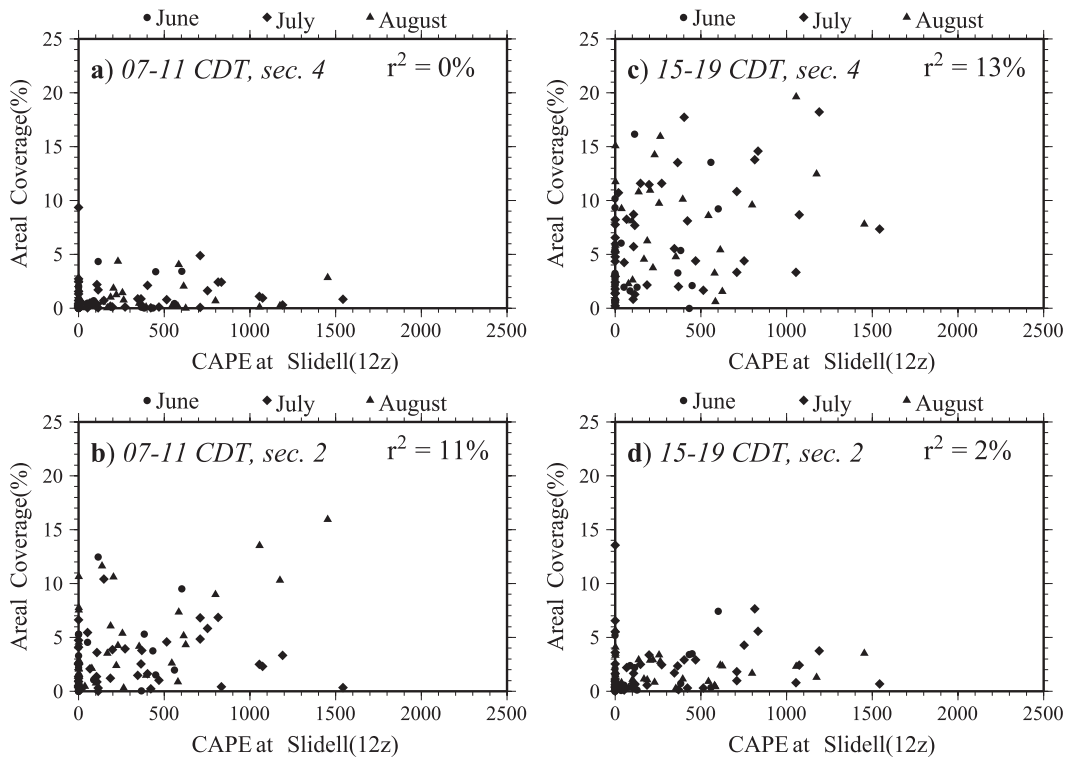


FIG. 16. As in Fig. 15, but for CAPE.

4. Discussion and conclusions

This study assesses the monthly climatology of the timing and placement of convective precipitation events induced by sea and land breezes in the Louisiana–Mississippi–Alabama region, and determines possible reasons for the monthly differences. These objectives were achieved through surface wind climatologies and radar composites, supplemented by a Wilcoxon rank sum test to identify statistically significant differences. The summer months of 2003–05 were screened for periods of minimal synoptic influence, identifying 102 “sea- and/or land-breeze” (SLB) days.

It is shown that, during the 3-yr period, June featured an easterly-to-southeasterly wind regime whereas July and August featured southerly flow. These wind regimes may have influenced monthly diurnal wind patterns along the coast. While all months featured a typical sea-breeze evolution, the local land breezes demonstrated monthly variations. July and August exhibit a westerly land breeze from eastern Louisiana, and the Mississippi land breeze tends to be stronger in August than in July. Calculations of ∇T support the observation that the sea- and land-breeze circulations along the Mississippi coast are stronger than those along the eastern Louisiana coast. Inertial forcing appears to make a contribution to the diurnal wind cycle in July and August within a southerly wind

regime. The daily wind speed minimum 50 km offshore from Mississippi indicates a local transition of influence from the land breeze to the sea breeze, and precedes the peak of the sea breeze at the coastline by about 2 h.

Overall, the radar composites follow the pattern of the local wind. During the nighttime hours, specifically between 2300 and 0700 CDT, precipitation is most prevalent offshore of the Louisiana coast, west of the Mississippi River, and especially over the Mississippi–Alabama Shelf region. By 1100 CDT, precipitation is observed over coastal regions, with a particular focus over southern Louisiana and near Mobile Bay. Local afternoon precipitation is widespread throughout the inland areas, while precipitation is minimal offshore.

Statistical significance tests of precipitable water (PW) and CAPE show that areal precipitation coverage (APC) increases in July and August on the Mississippi coast are due to more moist atmospheric layers and, to a lesser extent, additional instability. While PW variability certainly contributes to more widespread convection after June, greater offshore APC in July and August results from the influence of the local land-breeze setup. Convergence of a land breeze from eastern Louisiana and a stronger land breeze from Mississippi provides the additional lift needed to generate convection over a greater area. A stronger land breeze from Mississippi may lead to greater APC in August.

Multiple-regression analysis indicates that PW and CAPE each contribute to rainfall coverage variations—especially in the convectively active branches of the coastal density current—but much of the associated variance remains unexplained. The 850-hPa T_d , 850–500-hPa Γ , and 850-hPa wind direction are intermittently chosen in the stepwise regression, but often at lower significance levels. KI was seldom chosen and was rarely greater than the 90% significance level when selected, which is somewhat surprising since KI is widely perceived to be a good indicator of airmass thunderstorm coverage. Scatterplots indicate the upper percentile of the PW follows a linearly increasing trend for APC in the active radar sectors. Therefore, PW may be used to determine APC potential.

This study documents a climatological pattern of summertime convective precipitation, which may facilitate its prediction in the NCGC region. The unique combination of an irregular, west–east-oriented coastline, variant regional topography, relatively low latitude, daily conditional instability, and abundant moisture promotes the cycle of the SLB and associated convection in the NCGC region, with some monthly pattern variations.

Acknowledgments. This research is sponsored by the National Oceanographic and Atmospheric Administration (NOAA), with Grants NA060AR4600181 and NA050AR4601145, and through the Northern Gulf Institute, funded by Grant NA060AR4320264. The authors thank Dr. Haldun Karan for his careful review of the paper. Dr. Grady Dixon also provided feedback of the analysis work, and Kelsey Scheitlin contributed to the preparation of the manuscript. The National Weather Service of NOAA is the primary provider of surface observing data. RAWS hourly data were obtained from the USDA Joint Agricultural Weather Facility in Stoneville, Mississippi; these data are used specifically to assist with forecasting weather in fire-prone areas. Buoy data were obtained from the National Data buoy Center, the National Ocean Service, Louisiana State University, and the University of Southern Mississippi. David Walters of the U.S. Geological Survey provided meteorological data from Louisiana tide gauge stations. Multiple-regression calculations were performed using the International Mathematical and Statistical Library (IMSL). The Wilcoxon rank sum significance tests utilized the R software package.

APPENDIX

Is the K Index a Useful PoP Predictor?

The National Weather Service Operations Manual (NOAA 2005) defines probability of precipitation (PoP)

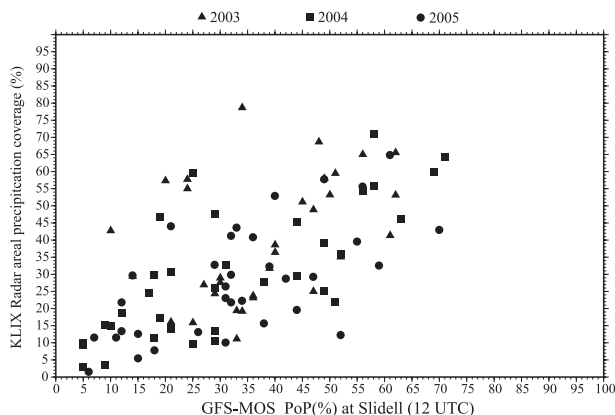


FIG. A1. The 1200 UTC GFS–MOS–predicted 12-h PoP for the sea-breeze case study days during 2003–05, plotted against the 1200–0000 UTC APC within 240 km of KLIX.

as the likelihood—expressed as a percent—of a measurable precipitation event *at any given point* within a forecast area and within a clearly stated time period. Schaefer and Livingston (1990) show that this definition of PoP can be interpreted as the expected areal coverage of precipitation (or APC) if a forecaster has complete certainty that a measurable precipitation event will occur somewhere within the forecast area. In the Louisiana and Mississippi Gulf coast area, airmass thunderstorms typically occur on most days in the summer; hence, the PoP could be interpreted to be the expected APC in the region, since forecasters will have high confidence of a rain event. To examine this assertion, the 12-h Global Forecast System–model output statistics (GFS–MOS) PoP forecast for Slidell, Louisiana, is plotted against the observed APC from the case study days (Fig. A1) for a 240-km circular area centered at Slidell. The result is a discernible linear trend of PoP to APC, with $r^2 = 39\%$ and a fairly even distribution of the scatter. The regression passes the constant variance test, and the residuals are distributed normally. This analysis suggests that the relationship of APC to PoP, promoted by Schaefer and Livingston (1990), is essentially valid.

The effectiveness of the association of the K index (KI) to APC was then investigated for this study. KI is a measure of airmass thunderstorm potential based on the temperature lapse rate, the moisture content of the lower troposphere, and the vertical extent of the moist layer, quantified by adding a sounding's 850-hPa T_d , 700-hPa dewpoint depression and the 850–500-hPa lapse rate (Γ). In this study, the 700-hPa dewpoint depression term correlated the most with KI (often $r^2 > 90\%$), while the lapse rate correlated the least ($r^2 \approx 10\%–15\%$). George (1960) originally proposed that an increase of KI corresponded with an increasing likelihood of airmass thunderstorm

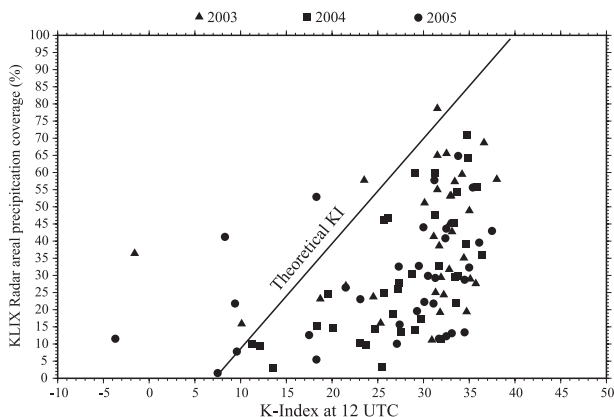


FIG. A2. KLIX KI at 1200 UTC for the sea-breeze case study days during 2003–05, plotted against APC from 1200 to 0000 UTC, centered at the KLIX radar out to 240 km. The solid line represents the theoretical KI relationship to APC.

development due to the dominance of the moisture terms in quasi-tropical environments. Theoretically, $KI = 15$ corresponds to $PoP = 20\%$, linearly increasing to 100% with $KI \geq 40$. However, the relationship of APC to KI for the daytime period of 1200–0000 UTC is weak within our study sample, with $r^2 = 20\%$ (Fig. A2). Furthermore, while the regression passes the constant variance test, it fails the normality test. The residuals are skewed positively, and a linear assumption may be invalid. $KI > 25$ represents a threshold where the APC could be large, but for most study days is less. Specifically, for $KI = 26$ – 30 , half of the study days have an APC of 25% or less, three-quarters are 33% or less, and $9/10$ ths are 50% – 60% or less. These percentiles do increase with KI. For $KI = 30$ – 35 , the 50th percentile margin of APC increases to 40% , the 75th percentile of APC is 54% , and the 90th percentile of APC is 64% . For $KI \geq 35$, these percentiles generally remain constant. Analysis of the nighttime period of 0000–1200 UTC revealed a similar trend for offshore convection (not shown), as did a regionalized analysis of sectors 1–4 (defined in Fig. 2) with 4-h analysis periods (not shown).

In short, only a weak relationship between KI and PoP was seen within our study sample, with the APC for most study days being significantly less than the theoretical value corresponding to the observed KI. However, it was noted that the 90th percentile of APC followed a linearly increasing trend for $KI < 35$.

REFERENCES

Anthes, R. A., 1978: The height of the planetary boundary layer and the production of circulation in a sea breeze model. *J. Atmos. Sci.*, **35**, 1231–1239.

Arritt, R. W., 1989: Numerical modelling of the offshore extent of sea breezes. *Quart. J. Roy. Meteor. Soc.*, **115**, 547–570.

Atkins, N. T., R. M. Wakimoto, and T. M. Weckwerth, 1995: Observations of the sea-breeze front during CaPE. Part II: Dual-Doppler and aircraft analysis. *Mon. Wea. Rev.*, **123**, 944–969.

Banta, R. M., L. D. Olivier, and D. H. Levinson, 1993: Evolution of the Monterey Bay sea-breeze layer as observed by pulsed Doppler lidar. *J. Atmos. Sci.*, **50**, 3959–3982.

Case, J. L., J. Manobianco, A. V. Dianic, M. M. Wheeler, D. E. Harms, and C. R. Parks, 2002: Verification of high-resolution RAMS forecasts over east-central Florida during the 1999 and 2000 summer months. *Wea. Forecasting*, **17**, 1133–1151.

—, M. M. Wheller, J. Manobianco, J. W. Weems, and W. P. Roeder, 2005: A 7-yr climatological study of land breezes over the Florida Spaceport. *J. Appl. Meteor.*, **44**, 340–356.

Colby, F. P., 2004: Simulation of the New England sea breeze: The effect of grid spacing. *Wea. Forecasting*, **19**, 277–285.

DeMaria, M., and J. Kaplan, 1994a: A Statistical Hurricane Intensity Prediction Scheme (SHIPS) for the Atlantic basin. *Wea. Forecasting*, **9**, 209–220.

—, and —, 1994b: Sea surface temperature and the maximum intensity of Atlantic tropical cyclones. *J. Climate*, **7**, 1324–1334.

Etherton, B., and P. Santos, 2008: Sensitivity of WRF forecasts for south Florida to initial conditions. *Wea. Forecasting*, **23**, 725–740.

Evans, J. L., 1993: Sensitivity of tropical cyclone intensity to sea surface temperature. *J. Climate*, **6**, 1133–1140.

Fovell, R. G., 2005: Convective initiation ahead of the sea-breeze front. *Mon. Wea. Rev.*, **133**, 264–278.

George, J. J., 1960: *Weather Forecasting for Aeronautics*. Academic Press, 673 pp.

Haurwitz, B., 1947: Comments on the sea-breeze circulation. *J. Meteor.*, **4**, 1–8.

Hawkins, J. D., 1977: A study of the mesoscale wind circulation in a land-sea breeze regime. *Bull. Amer. Meteor. Soc.*, **58**, 1289–1295.

Lu, D., L. White, R. S. Reddy, P. J. Croft, and J. M. Medlin, 2006: Numerical simulation of sea and bay breezes in a weak shear environment. *Meteor. Atmos. Phys.*, **94**, 153–165.

Lu, R., and R. P. Turco, 1994: Air pollutant transport in a coastal environment. Part I: Two-dimensional simulations of sea-breeze and mountain effects. *J. Atmos. Sci.*, **51**, 2285–2308.

McPherson, R. D., 1970: A numerical study of the effect of a coastal irregularity on the sea breeze. *J. Appl. Meteor.*, **9**, 767–777.

Medlin, J. M., and P. J. Croft, 1998: A preliminary investigation and diagnosis of weak shear summertime convective initiation for extreme southwest Alabama. *Wea. Forecasting*, **13**, 717–728.

Neumann, J., 1951: Land breezes and nocturnal thunderstorms. *J. Atmos. Sci.*, **8**, 60–67.

NOAA, 2005: WFO public weather forecast products specification. National Weather Service Instruction 10-503, NWS, 75 pp. [Available online at <http://www.nws.noaa.gov/directives/010/archive/pd01005003b.pdf>.]

Physick, W. L., and R. A. D. Byron-Scott, 1977: Observations of the sea breeze in the vicinity of a gulf. *Weather*, **32**, 373–381.

Pielke, R. A., 1974: A three-dimensional numerical model of the sea breezes over south Florida. *Mon. Wea. Rev.*, **102**, 115–139.

Ramis, C., A. Jansa, and S. Alonso, 1990: Sea breeze in Mallorca. A numerical study. *Meteor. Atmos. Phys.*, **42**, 249–258.

- Reap, R. M., 1994: Analysis and prediction of lightning strike distributions associated with synoptic map types over Florida. *Mon. Wea. Rev.*, **122**, 1698–1715.
- Reimann, C., P. Filzmoser, R. Garrett, and R. Dutter, 2008: *Statistical Data Analysis Explained: Applied Environmental Statistics with R*. John Wiley and Sons, 362 pp.
- Rotunno, R., 1983: On the linear theory of the land and sea breeze. *J. Atmos. Sci.*, **40**, 1999–2009.
- Schaefer, J. T., and R. L. Livingston, 1990: Operational implications of the “probability of precipitation.” *Wea. Forecasting*, **5**, 354–356.
- Sheng, C., M. Xue, and S. Gao, 2009: The structure and evolution of sea breezes during the Qingdao Olympics sailing test event in 2006. *Adv. Atmos. Sci.*, **26**, 132–142.
- Simpson, J. E., 1994: *Sea Breeze and Local Winds*. Cambridge University Press, 234 pp.
- Smith, J. R., H. E. Fuelberg, and A. I. Watson, 2005: Warm season lightning distributions over the northern Gulf of Mexico coast and their relation to synoptic-scale and mesoscale environments. *Wea. Forecasting*, **20**, 415–438.
- Steiger, S. M., and R. E. Orville, 2003: Cloud-to-ground lightning enhancement over southern Louisiana. *Geophys. Res. Lett.*, **30**, 1975, doi:10.1029/2003GL017923.
- Steyn, D. G., and I. G. McKendry, 1988: Quantitative and qualitative evaluation of a three-dimensional mesoscale numerical model simulation of a sea breeze in complex terrain. *Mon. Wea. Rev.*, **116**, 1914–1926.
- Wakimoto, R. M., and N. T. Atkins, 1994: Observations of the sea-breeze front during CaPE. Part I: Single-Doppler, satellite and cloud photogrammetry analysis. *Mon. Wea. Rev.*, **122**, 1092–1114.
- Wilcoxon, F., 1945: Individual comparisons by ranking methods. *Biometrics*, **1**, 80–83.
- Wilson, J. W., and D. L. Megehard, 1997: Thunderstorm initiation, organization, and lifetime associated with Florida boundary layer convergence lines. *Mon. Wea. Rev.*, **125**, 1507–1525.